DEGREE PROJECT, IN NANOTECHNOLOGY , SECOND LEVEL
STOCKHOLM, *SWEDEN 2015*

Hexosomes as drug delivery vehicles for antimicrobial peptides

SZYMON SOLLAMI DELEKTA

KTH ROYAL INSTITUTE OF TECHNOLOGY

ICT SCHOOL

Hexosomes as drug delivery vehicles for antimicrobial peptides

Szymon Sollami Delekta

Supervisor: Lukas Boge

Examiner: Mark Rutland

Abstract

This master thesis project was carried out at SP Technical Research Institute of Sweden within the FORMAMP project which goal is to increase the efficiency and stability of antimicrobial peptides (AMPs) by exploring and developing a number of innovative formulation strategies for the drug delivery of those systems. In view of the growing problem of bacterial resistance to traditional antibiotics, AMPs represent one of the most promising alternatives as therapeutics against infectious diseases: besides having a fast and non-specific mechanism of action, they are less prone to bacterial resistance.
In this project, the goal was to develop an efficient method for the formulation of hexagonal lyotropic phase nanodispersions (called hexosomes) as drug delivery vehicles for the AP114, DPK-060 and LL-37 AMPs. Then, these formulations were characterized through size measurements, zeta potential measurements, SAXS, cryo-TEM and UPLC and their stability was assessed. Lastly, the interaction of these systems with model bacterial membranes was tested through QCM-D and ellipsometry.

The relevant samples were found to have a hexagonal structure with the lattice parameter being larger when peptide was loaded. The systems were observed to be sufficiently stable and the peptide loading efficiency was found to be higher than 90% in most cases. The hexosomes loaded with LL-37 were observed to preserve the effectiveness of the peptide when interacting with the model membrane through QCM-D.

Nomenclature

AP114	H_2N-GFGCNGPWNEDDLRCHNHCKSIKGYKGGYCAKGGFVCKCY
AMP	Antimicrobial peptide
CMC	Critical micelle concentration
CPP	Critical packing parameter
DLC	Dynamic light scattering
DOPE	1,2-dioleoyl-sn-glycero-3-phosphoethanolamine
DOPG	1,2-dioleoyl-sn-glycero-3-phospho-(1'-rac-glycerol)
DPK-060	GKHKNKGKKNGKHNGWKWWW
GMO	Glycerol monooleate
LC	Liquid crystal
LCNP	Liquid crystalline nanoparticle
LL-37	LLGDFFRKSKEKIGKEFKRIVQRIKDFLRNLVPRTES
MIC	Minimum inhibitory concentration
OA	Oleic acid
Phyt	Phytantriol

Contents

Chapter 1

Introduction

In 1897 Ernest Duchesne, a 23 year old French student, found out that guinea pigs infected with *Salmonella typhi* or *Escherichia coli* could be cured by injecting them with mould (*Penicillium glaucum*). Since then antibiotics have gone a long way. In 1909 Paul Ehrlich developed Salvarsan for curing syphilis, in 1928 Alexander Fleming synthesized penicillin which treated serious bacterial infections caused by *streptococci* and *staphylococci*. The first synthesized sulfonamide became the first commercially available antibacterial agent (Prontosil) and started a 20 year period in the 50's called the golden era of discovery of new antibiotics classes[1]. Unfortunately Duchesne was not as lucky: his thesis was refused, his work forgotten for many years and he died aged 37 probably from (ironically enough) tuberculosis[2].

Eventually, antibiotics became so widespread during the 60's that any minor ailment entailed a shot of antibiotic by the doctor "just in case" and farm animals received antibiotics regularly for a faster growth[3]. The overuse and misuse of antibiotics causes them to be released in large quantities in the environment and causes bacteria to be exposed to them. As a result, a threatening situation has arisen where alarming numbers of bacteria have developed antibiotic resistance. According to a World Health Organization report from 2014:

"Antimicrobial resistance (AMR) within a wide range of infectious agents is a growing public health threat of broad concern to countries and multiple sectors. Increasingly, governments around the world are beginning to pay attention to a problem so serious that it threatens the

achievements of modern medicine. A post-antibiotic era — in which common infections and minor injuries can kill — far from being an apocalyptic fantasy, is instead a very real possibility for the 21st century[4].”

Before the introduction of Penicillin, the mortality caused by a *Staphylococcus aureus* bacteremia exceeded 80%[5, 6]. Even though at first the antibiotic dramatically reduced this rate, by the 60’s more than 80% of the *S.aureus* isolates were already resistant to Penicillin. In an attempt of improving patients´ prognoses, Methicillin was introduced but soon it inevitably became ineffective as well when the *S. aureus* became Methicillin-resistant (MRSA). Nowadays MRSA has developed resistance against most antibiotics and is the reason for most of the hospital-acquired infections.

Probably the most significant example of the impact of the bacterial resistance is tuberculosis (TB) caused by *Mycobacterium tuberculosis* (MTB). In 2012 1,3 million people died as a result of tuberculosis and one estimates that 170 000 deaths were caused by drug-resistant TB (DR-TB) globally[4]. Drug resistance in TB is a major public health problem in many countries due to the fact that it is increasingly difficult to treat it properly. While drug susceptible TB is treated in 6 months with a combination of 4 conventional antibiotics, DR-TB requires 20 months or longer and daily administration of drugs which are less effective and have more side effects. Among other more or less drug resistant pathogens worth mentioning are *Shigella* causing annually 1 million deaths worldwide, *S. pneumoniae* targeting infants and elders and most common cause of meningitis and nontyphoidal *Salmonella* causing annually 150 000 deaths on a global scale[4]. *Escherichia coli* is an other example and even though it is part of the intestinal flora, it is the most frequent case of hospital and community-acquired urinary infections, blood stream infections and meningitis in neonates. A report shows that in the USA more than 63 000 patients die every year from hospital acquired bacterial infections[7, 1].

It seems that when an antibiotic is introduced it is a matter of time before resistance is developed so research is forced to frenetically rush with the discovery and development of new antibiotics. As a result, new countermeasures and alternatives are being investigated, one of

the most promising being antimicrobial peptides.

The aim of this thesis is to investigate the possibility of including antimicrobial peptides into drug delivery systems constituted by hexagonal liquid crystalline phases. Such vehicles have the potential of improving the effectiveness of these drugs and avoiding typical problems connected to their administration.
The evaluation of the hexagonal structures will be performed through characterization techniques while their interaction with specific targets will be studied through interfacial sensing techniques.

Chapter 2

Theoretical background

2.1 Antimicrobial peptides (AMPs)

Antimicrobial peptides are part of the innate host defense effector molecules which have been isolated and characterized from species of all kingdoms[8]. In a broad sense the term antimicrobial peptide refers to all peptides that are capable of killing targeted bacteria (or inhibit their growth), viruses and fungi. AMPs also have roles as mediators of inflammation on epithelial and inflammatory cells giving benefits such as immune induction, cell proliferation, wound healing and cytokine release. AMPs can be oligo- or polypeptides which are formed by short chains of amino acids linked by amide bonds (peptide bonds)[9].
More than 2500 AMPs have been isolated[10]. Their classification is not straightforward due to the variety of structures, origin, mechanisms and functions.

Even though AMPs are greatly diversified, they share few common features such as cationicity, amphiphilicity and sequences not longer than 50 amino acids. They are classified in four structural groups[11]: peptides with a cationic α-helical linear structure, peptides with β-sheet structures containing disulphide bonds, peptides with predominance of one or more amino acids and peptides with loop structures[12].
The most notable feature of AMPs is the ability to successfully target pathogens by having a preferential affinity and specificity for microorganisms rather than mammalian cells. The property was extensively tested and demonstrated in vivo with the study performed by *Welling*

et al. Synthetic labelled derivatives of human ubiquicidin and lactoferrin were intravenously injected into animals infected with *K. pneumoniae* and *S. aureus*. In the study AMPs were successfully observed to aggregate in infected tissues while at the same time showing no signs of aggregation in sterile inflammations[13].

Due to the novelty of those systems, there is a small number of studies supplying information about their antigenicity, immunogenicity, toxicity, their behaviour in physiological conditions and eventual intrinsic side effects. Furthermore, AMPs were observed to be sensitive to high ionic strength, susceptible to proteolysis and carry high production costs[11, 14].
In general, the action of AMPs is dependent on some of their properties[15, 16, 17, 18]:

- Chain length: with increasing peptide length, affinity to the bacterial membrane is promoted and the tendency to form amphiphilic secondary structures increases. This results in a higher antimicrobial effect as some studies confirm[19, 20].

- Charge: the penetration through peptide-disrupted membranes generally increases with increasing AMPs positive net charge[21, 22]. Bacterial membranes are usually negatively charged so the electrostatic attraction is higher for more positively charged peptides. Due to the zwitterionic nature of most AMPs, the pH of the solution plays a role in the process too.

- Secondary structure: particular ordered structures such as α-helical structures facilitate membrane disruption according to some studies[23, 24, 18]. However, for a number of AMPs the helicity factor is less important[25].

- Hydrophobicity: increased hydrophobicity of the peptide was found to aid membrane disruption because it avoids electrostatic screening effects caused by high ionic strength occurring at physiological conditions[21, 22, 17]. However, an increased hydrophobicity causes a higher toxicity as well.

2.1.1 Mechanisms of action

As already introduced, AMPs possess a variety of properties which allow them to exert a multitude of actions within the immune system. The most obvious action is the antimicrobial activity and they are able to target both Gram-positive and Gram-negative bacteria.
Electrostatic interactions between the positively charged peptides and the negatively charged bacterial membrane enable the initial binding and accumulation with various orientations on the surface. When a specific concentration is reached AMPs are prompted to modify the biophysical properties of the targeted membrane[11] resulting in a disruption of the membrane and consequently to the death of the organism.
The MIC (minimum inhibitory concentration) is one of the most used test to compare the efficiencies of antibiotics and AMPs in vitro[12]. It is a parameter which depends on peptide charge, hydrophobicity, amphiphaticity, composition and peptide´s likeliness to self-assembly[14].

Membrane disruption is a process which kills bacteria by virtue of the leakage of intracellular components. Three disruption models were proposed and are generally accepted by the scientific community. However, they may be too rigid to explain fully the multitude of phenomena involved and a concurrence of some is most likely to happen[12]. The three models as described in [12, 17, 18, 15] are:

- Barrel-stave pore model (or helical bundle model): AMPs approach the membrane as monomers or oligomers with an α-helical structure and penetrate perpendicularly[24, 12]. Upon association, their hydrophobic surfaces bind to the lipid bilayer while the hydrophilic regions remain exposed thus forming a transmembrane pore in the bilayer consisting of at least 4 peptides. As a consequence, additional peptides are likely to aggregate in the channel leading to a pore diameter increase. This model was first proposed by *Ehrenstein and Lecar* in 1977[26] and was observed in only few AMPs (such as alamethicin) because of its requirements in terms of peptide properties[14]. See Figure 1a.

- Carpet mechanism: AMPs accumulate, cover carpet-like the membrane and then orientate parallel to the surface. The hydrophobic regions face the membrane while the hydrophilic regions are exposed to the solvent. Once a certain surface coverage of bound

peptide is reached, peptides start disrupting the membrane in a detergent-like manner thus leading to the formation of micelles[27]. See Figure 1b.

- Toroidal pore model: at first AMPs accumulate parallel to the surface and then either penetrate perpendicularly the membrane or induce a curvature in the membrane leading to an opening caused by strain (called toroidal pore). Upon approach of even more peptides, either the membrane could be disrupted and micellized in a detergent-like mechanism or peptides could traverse the membrane and reach the inner leaflet[24]. The toroidal pore formation was demonstrated for a big variety of peptides. See Figure 1c.

However, it must be mentioned that not all peptides make use of these bactericidal mechanisms. For instance the antimicrobial peptide plectasin targets the cell wall (see Section 2.1.4).

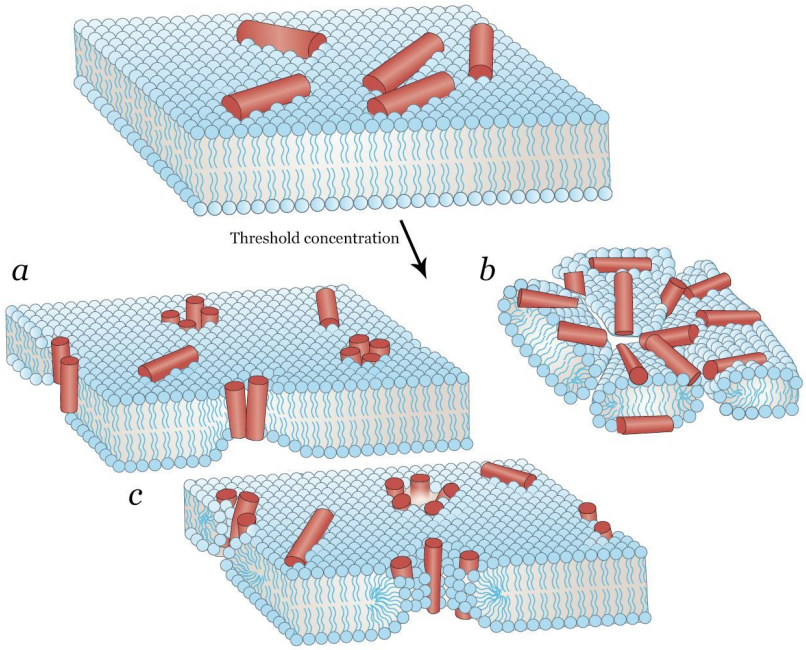

Figure 1: *Membrane disruption models. a)Barrel-stave pore model; b)Carpet mechanism; c)Toroidal pore model[12].*

The three AMPs investigated in this work are LL-37, DPK-060 and AP114 and they are briefly described below.

2.1.2 LL-37

The LL-37 antimicrobial peptide belongs to the group of cationic α-helical linear peptides. It is the only human antimicrobial peptide in the cathelicidin family[28] and is isolated from human bone marrow[11]. It constitutes the C-terminal part of the hCAP18 cathelicidin protein. Its amino acid sequence is LLGDFFRKSKEKIGKEFKRIVQRIKDFLRNLVPRTES, the M_w is 4490,7 Da and the secondary structure is α-helix upon interaction with the membrane. The peptide is found in a number of different cell types and tissues such as skin, lungs, nasal mucosa and saliva.

LL-37 actively targets both Gram-positive and Gram-negative bacteria and is extensively studied as a drug development candidate. Several properties such as broad-spectrum bacterial activity at physiological concentrations make it particularly interesting[29]. Besides the antimicrobial activity. LL-37 and other mammalian cationic host defense peptides have other noteworthy functions such as effectiveness against pathogens such as fungi and viruses, anti-endotoxin activity, chemotacticity, influencing cell proliferation and differentiation, have wound healing properties and angionogenesis promotion and selective modulation of pro-inflammatory responses[30]. The peptide is sensitive to proteolytic degradation.

2.1.3 DPK-060

DPK-060 is a novel clinical stage antimicrobial peptide developed by Pergamum AB and is derived from the endogenous human protein kininogen[31]. The amino acid sequence is GKHKNKGKKNGKHNGWKWWW, M_w is 2503,4 Da and the secondary structure is a random coil. It is intended for topical administration and its main applications are treatment of chronic wounds, prevention of scars and adhesions and anti-infective treatments[32].

From a clinical Phase II study (double-blind, randomized, placebo-controlled trial) performed on patients with acute external otitis DPK-060 has proved to be effective[33]. Also, a second clinical study on atopic dermatitis has showed positive data hinting that DPK-060 is able to potentially treat a span of dermatological conditions.

As for the antimicrobial properties, it targets a broad spectrum of pathogens, ranging from Gram-Positive (such as *S. aureus*) and Gram-negative bacteria to fungi (*Candida* and

Malassezia). It is sensitive to chemical degradation.

2.1.4 AP114

AP114 (previously known as NZ2114) is an antimicrobial peptide derived from plectasin, a 40-amino acido defensin produced by the fungus *P. nigrella* and developed by Novozymes. The amino acid sequence is H_2N-GFGCNGPWNEDDLRCHNHCKSIKGYKGGYCAKGGFVCKCY, M_w is 4407,9 Da and the structure is a Cystine-stabilized α/β-fold. Contrary to the bactericidal mechanisms of most of the AMPs, plectasin acts by binding to Lipid II, a bacterial cell wall precursor, thus inhibiting its cell wall biosynthesis.
AP114 is strongly active against Gram-positive bacteria such as *streptococci*, including PSSP (*Penicillin-susceptible S. aureus*) and PRSP (*penicillin-resistant S. aureus*), and *staphylococci*, including the methicillin-resistant MRSA and the vancomycin-resistant VRSA[34, 35]. Targeted diseases and conditions include skin infections, pneumonia, septicemia and endocarditis.

Furthermore, plectasin shows extremely low toxicity in mice and has a high therapeutic potential due to its effectiveness.

2.1.5 Bacterial resistance to AMPs

Thanks to the nature of their mechanism of action exploiting features of the bacterial membrane, AMPs are considered one of the most promising counteractions to the rising threat of antibiotic resistance since they were discovered[36]. Besides their antimicrobial, antiviral, antifungal and antitumoral features, AMPs have a multitude of functions in the immune system: they can promote leukocyte recruitment in infection sites, induce wound healing mechanisms, generate vascular systems, prevent obesity development and induce cell differentiation processes[14].
Some AMP resistance mechanisms were reported, the most frequently described mechanism being bacterial cell surface alteration. *S. aureus* can add L-lysine or L-alanine to phosphatidylglycerol in the cell membrane to increase the positive net charge[37] or it modifies cell membrane phospholipids with the same scope, *Salmonella* amidates Lipid A constituents in order to hinder electrostatic interactions[8].

Regardless of the bacterial resistance mechanism, the practical advantage of AMPs over traditional antibiotics is twofold, extremely high diversity, variety of structures and mechanisms of action being the first and high target specificity being the second. In the past 50 years most traditional antibiotics have become nearly ineffective within the first years since introduction on the market while natural AMPs have remained functional despite bacteria having been continuously exposed to such bactericidal agents. In order to develop any form of resistance, bacteria need to redesign their membrane, changing both organization and composition of lipids which is an impractical solution[23].

Even though in the near future a rapid evolution of AMP resistance is unlikely to be developed, the use of artificially synthesized AMPs constitutes concern and needs to be further studied and evaluated[23, 36].

2.2 Liquid crystalline structures

Liquid Crystals (LCs) are structures which exhibit common features and physical properties of liquids and solids so, for instance, they may possess a partial order of atomic species while still presenting a flow typical of liquids[38].
LCs are encountered in many aspects of our everyday life: they are largely used in flat panel displays and lasers due to their optical properties, cell membranes are liquid crystalline phases created by phospholipids dissolved in water[39] and even many detergents and soaps in water form liquid crystals[40].

The physical processes governing the formation of LCs provide a first classification of the liquid crystalline phases: thermotropic and lyotropic.
The thermotropic class refers to the liquid crystal phases formed by a temperature change. If a chemically pure material melts over an interval of temperatures thus giving a gradual transition, the material is expected to exhibit a liquid crystal structure over that range. The formation of LCs cannot happen when the melting transition is an abrupt process and the stability is a

function of temperature. These are the most commonly used liquid crystals mainly due to their linear and nonlinear optical properties.
Lyotropic LCs are formed through the dissolution of a solute in a solvent (usually water) and the structures studied in this thesis belong to this category. The molecules which generate lyotropic liquid crystals are amphiphilic: they possess both polar and non-polar regions or in other words they have an amphipathic character[40]. Amphiphilic molecules (generally surfactants) are constituted by a polar head group which can be anionic, cationic, nonionic or zwitterionic with a non-polar chain connected. The heads are hydrophilic while the tails are hydrophobic. Due to this ambivalent character, in water they tend to self-assemble into aggregates with different micellar structures in order to protect the hydrophobic tails from coming into contact with water. The minimal concentration at which micelles start forming is called the critical micelle concentration, CMC[41]. Being spherical isotropic structures, micelles act as elementary units for the formation of the following lyotropic phases: lamellar, cubic, hexagonal, nematic, gel and intermediate[42].

Liquid crystalline phases are often dispersed to form dispersions of particles at the sub-micrometer scale.
According to past research, the dispersed phase preserves the internal structure of the bulk phase and additionally it brings some new beneficial properties. Exhibiting high fluidity, its practical application is significantly easier and it can be incorporated into other formulations. Furthermore, the large surface area of the micro and nanoparticles enhances their interaction with the skin and other surfaces thus increasing drug delivery efficiency[43].

2.2.1 Lamellar phases

Lamellar phases consist of amphiphilic molecules self-assembled into bilayers extended at a large distance and alternated with water layers. The non-polar tails from the two opposite sides intertwine with each other. The water layer thickness is usually between 1 and 10 nm with water content between 10% and 50% by weight[40] and the thickness of the layers is usually less than twice the length of each amphiphile[44]. These structures are the most common in lyotropic

crystals. If dispersed, the lamellar phases are called liposomes.

2.2.2 Cubic phases

There are 2 types of cubic phases: discontinuous (I type) and bicontinuous (V type). The first group consists of either primitive (Pm3n space group), normal face centered (Fm3m), reverse face centered (Fd3m) or body centered (Im3m) cubic lattices built up by regularly packed globular micelles. Bicontinuous cubic phases consist of aggregated curved bicontinuous lipid bilayers assembled in an infinite periodic minimal surface. Three bicontinuous periodic structures have been identified: a primitive lattice (Pn3m) and two body-centered lattices (Ia3d and Im3m)[42, 39, 45]. Those phases are highly viscous, difficult to handle[46] and if dispersed are called cubosomes.

2.2.3 Hexagonal phases

Hexagonal phases are formed by rod-like micelles packed together. The two dimensional micelles arrange into a hexagonal lattice so each micelle is surrounded by six others. Two different hexagonal structures exist.
H_1 is the normal hexagonal phase in which the inner volume of each micelle is hydrophobic tails with polar head groups facing outwards. H_2 is the reverse hexagonal phase which has micelles with an inner volume containing the hydrophilic polar head groups. H_1 is water continuous and H_2 is alkyl chain continuous instead. Their formation is discriminated by the CPP as explained in Section 2.3. If hexagonal phases are dispersed they are called hexosomes. Hexagonal phases will be the main focus of this thesis.

2.2.4 Other phases

A number of other liquid crystalline phases exists. For instance, nematic phases consist of micelles assuming the shape of rods or columns with their long dimension oriented towards a preferred direction. Gel phases are formed by amphiphilic bilayers similarly to lamellar phases but they have highly regular intermolecular arrangements which increase their viscosity[42].

2.3 The Critical Packing Parameter (CPP)

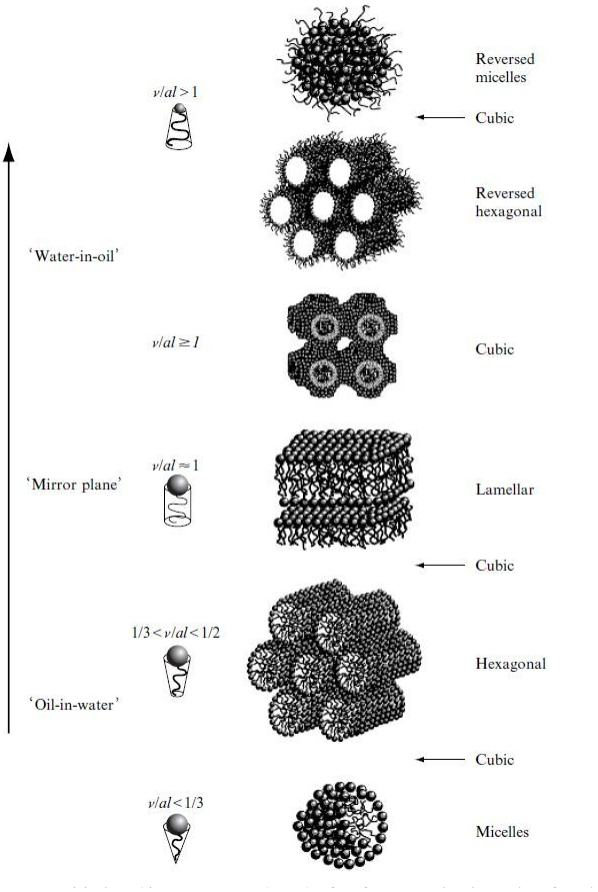

Figure 2: *Liquid crystalline structures and the CPP[46].*

The liquid crystalline structure which the molecule is most likely to form depends on a geometrical model based on the CPP of the surfactants involved. The CPP of a surfactant is a dimensionless number relating the volume of its alkyl chain (v), its extended length (l_{max}) and its head group area (a)[46]:

$$CPP = \frac{v}{l_{max} a} \tag{1}$$

Figure 2 summarizes CPP values and the corresponding lyotropic structures helping at the same time to visualize the geometries involved in this section.

The CPP depends on parameters such as lipid polarity, temperature, amount of water and addition of hydrophilic or hydrophobic amphiphilic molecules[47].

2.4 The hexagonal phase as a drug delivery vehicle

Drug delivery vehicles are researched primarily due to their ability of trapping, encapsulating, transporting and releasing active pharmaceutical ingredients, thus increasing the drug efficiency. This leads to an overall dose reduction and reduced toxicity. Reportedly hexagonal phases exhibit interesting properties as drug delivery systems when compared to other liquid crystalline structures. They can be loaded with large molecules such as peptides and proteins, enhance drug penetration through skin as assessed by *in vitro* models, allow a high drug loading and may protect the loaded drug from physical and enzymatic degradation[47, 43].

A number of amphiphilic compounds (surfactants) is capable of forming a liquid crystalline structure in aqueous solution at physiological conditions and room temperature. In literature the most studied material for creating such phases is glycerol monooleate (GMO) and its variations such as diglycerol monooleate (DGMO)[46, 39]. Phytantriol (3,7,11,15-tetramethyl hexadecantriol, Phyt) is a cosmetic ingredient which shows similar phase behaviour to GMO[48] and was also researched as drug delivery candidate. Other compounds are oleyl glycerate (OG) and phytanyl glycerate (PG) which, however, were scarcely studied for these applications.
In order to form hexagonal phases, nonpolar additives such as oleic acid (OA), triacyl glycerol, tetradecane and vitamin E acetate may need to be added. In some systems an increase in temperature is also required[47].

In the case in which the lyotropic phase is not bulk but dispersed in solution, the most commonly employed stabilizers are amphiphilic triblock copolymers (poloxamers) such as pluronic F127. These stabilizer molecules are constituted by separated hydrophobic and hydrophilic chains so the reason why F127 stabilizes effectively GMO nanoparticles is that the hydrophobic regions of the poloxamer's amphiphiles penetrate into the internal structure of the nanoparticle through the water channels thus shielding it from neighbouring nanoparticles and preventing their aggregation. In the case of hexosomes, the poloxamer is located mainly at the outer surface as the aqueous channels are too narrow to allow the poloxamer to penetrate[49]. The result of the steric stabilization is that the particle size diameter remains constant over time. Although

the nature of the interactions of pluronic F127 with Phyt and the over systems is little known[48], its effect on Phyt systems was found to be much more weak[50].

2.5 Nanostructured materials as AMP delivery systems

To the best of our knowledge, no research on the incorporation of AMPs onto neither bulk nor nanodispersed hexagonal LC phases was performed to date. However, studies on LCNPs as drug delivery vehicles for insulin[51], ovalbumin[52, 53, 54, 55], somatostatin[56] and cyclosporine A[57, 43] are present in literature and they employ mainly cubosome nanoparticles.
The main goal of using LC colloids as peptide delivery systems is to protect peptides from proteolysis which could otherwise degrade before it reaches the target. Susceptibility to proteolytic degradation can be very different from one peptide to another: LL-37 is very likely to be degraded so an improvement in proteolytic stability is decisive[58], while for DPK-060 the main issue is chemical stability. The administration area plays a role too, in infected wounds or airways the proteolytic activity is very high. Also, LCNP loading improves chemical stability by shielding the peptide from deamidation which is a common problem for AMPs.
Furthermore, LCNPs can be used to trigger and control peptide release. In some applications such as pulmonary and skin infection treatment, a supported and constant release of AMP over time enables the local administration of relatively higher doses without causing toxicity due to the presence of an excessive amount of peptide in the system.
Lastly, nanocarriers can be used to improve formulation functionality and to provide secondary beneficial effects by i.e. enhancing skin penetration, combining multiple formulations, absorbing excess fluids in wounds, improving skin hydration and increasing bioavailability[57, 59, 60].

2.6 Formulation components

For this project the GMO/OA and Phyt/OA systems were chosen. The reasons for such choice are mostly practical. According to literature few process steps are required to formulate such hexosomes and the formulation can be performed at room temperature. Those compounds are also widespread and easy to obtain.

2.6.1 Glycerol monooleate

GMO is a glycerol fatty acid ester (see Figure 3). An ester bond binds together the glyceryl backbone and the acyl chain. The glycerol headgroup has hydrophilic behaviour and can form hydrogen bonds with water. It is non-toxic, biodegradable and biocompatible and is included in the Handbook of Pharmaceutical Excipients[61].

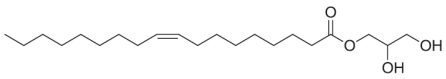

Figure 3: *Glycerol monooleate[45].*

GMO is nowadays mainly used in the production and stabilization of emulsions and foams in cakes, margarine and chewing gums. The reason for it being so widespread in pharmaceutics is its absorption enhancing properties in the *stratum corneum*[39].

2.6.2 Phytantriol

Being mostly used for hair care, skin and nail preparations[62] this long-chained polyol (see Figure 4) was recently proposed as a good alternative to glyceride lipids for the preparation of liquid crystalline phases. Phytantriol has 3 hydroxyl headgroups and a highly branched Phytanyl tail. It is highly viscous at room temperature.

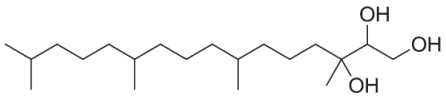

Figure 4: *Phytantriol[45].*

Unlike GMO it does not contain an ester bond, which makes it less susceptible to chemical degradation. Nonetheless, Phyt has a similar phase behaviour: it forms a bicontinuous cubic phase in excess water at room temperature while at higher temperatures a reversed hexagonal phase[48, 63].

Phytantriol is being investigated as a potential alternative for hexosome and cubosome preparation mainly due to its relatively high chemical stability and purity compared to GMO systems but information about this system is limited especially in the dispersed case.

2.6.3 Oleic acid

Oleic acid is a fatty acid (see Figure 5). It is odourless, yellowish and an oily liquid at room temperature. It can be easily obtained from olive oil which is its primary source. Oleic acid is used as an emulsifying agent in foods and in both cosmetic and pharmaceutical topical formulations. OA is also a penetration enhancer, it is biocompatible and is included in the Handbook of Pharmaceutical Recipients[61].

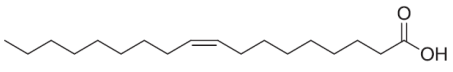

Figure 5: *Oleic acid[45].*

2.7 Applications of the formulations

The main administrations of the nanocarrier systems described in this work are topical.
Besides the already mentioned advantages, hexosome nanoparticles have the potential of being highly efficient as topical delivery vehicles thanks to the high surface area and low viscosity. In a study by *Lopes et al.*[43] hexosomes were also demonstrated to increase *in vitro* skin penetration of vitamin K and large peptide cyclosporine A. This beneficial effect is probably due to the presence of GMO and OA in the formulations (see Section 2.6.1 and Section 2.6.3) which are penetration enhancers allowing the drug to penetrate the *stratum corneum* and even deeper skin layers to some extent. Enhanced skin penetration could also be depending on the complexity of the structure but the factors and interactions involved are still not fully understood.
In the same study, the lack of adverse side effects of hexosomes was assessed during topical administration. Nanodispersions were demonstrated to not cause skin irritation for up to 2 days by evaluating parameters such as epidermal thickening, edema and immunocyte infiltration[43].

2.8 Bacterial membranes

All cells and bacteria have an outer bacterial membrane which is critical for survival as it constitutes a selective barrier which both isolates the bacteria or cell from the environment and allows specific molecules to travel across. The reason behind AMP specific bacterial membrane targeting is the inherent difference in structures and compositions between eukaryotic cell and bacterial membranes. A eukaryotic cell membrane consists of a bilayer of phospholipids populated by globular proteins, glycoproteins, protein channels, surface proteins and cholesterol which accounts for up to 45% of the total lipid composition[15, 64].
Bacteria instead are divided into Gram-positive and Gram-negative bacteria, none containing cholesterol. Gram-positive bacterial membranes are composed of a single phospholipid bilayer covered by a polymeric matrix called peptidoglycan which includes strains of teichoic acid. Gram-negative bacteria instead are constituted by two phospholipid bilayers (the outer being bounded to lipopolysaccharides (LPS) via Lipid A) separated by a layer of peptidoglycan. Figure 6 provides a summary of the structures.

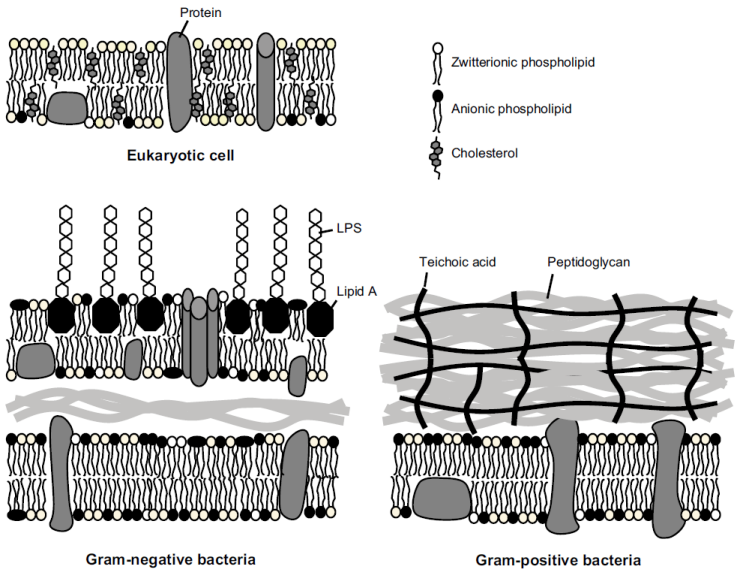

Figure 6: *Schematic depiction of the structure of eukaryotic cells, Gram-negative and Gram-positive bacteria[15].*

The bacterial membrane composition is unique in each bacterial strain and is also affected by factors such as exposure to antibiotics and changing environment[65]. The most common

molecules found in target cytoplasmic membranes are phosphatidylglycerol (PG), cardiolipin (CL, or diphosphatiglycerol, DPG)[15] and phospatidylethanolamine (PE). Such compositions are usually expressed as binary systems with w/w ratios. Examples of Gram-positive bacteria are *S. aureus* and *S. pneumonia* containing 50:50 CL/PG, *K. pneumonia* and *P. mirabilis* containing 80:20 PE/PG[65]. In the case of *E. coli* the outer membrane contains 91:3:6 PE/PG/DPG while the inner membrane contains 82:6:12 PE/PG/DPG[15].

2.9 Membrane models

In order to understand the mechanism of action of the formulations and to assess their effectiveness, it is fundamental to utilize manageable model bacterial membranes instead of complex bacterial surfaces. A number of phospholipids was used in literature, namely 1,2-dimyristoyl-sn-glycero-3-phosphocholine (DMPC), 1-palmitoyl-2-oleoyl-sn-glycero-3-phosphocholine (POPC), 1,2-dimyristoyl-sn-glycero-3-phosphoglycerol (DMPG), 1-palmitoyl-2-oleoyl-sn-glycero-3-phosphoglycerol (POPG), 1-palmitoyl-2-oleoyl-sn-glycero-3-phosphoethanolamine (POPE), 1,3-bis(sn-3'-phosphatidyl)-sn-glycerol (CL). In most of these studies, a combination of these lipids was used[65].

In this thesis, the phospholipids needed to emulate a simple bacterial membrane constituted by PE and PG. The chosen phospholipids were 1,2-dioleoyl-sn-glycero-3-phosphoethanolamine (DOPE) and 1,2-dioleoyl-sn-glycero-3-phospho-(1'-rac-glycerol) (DOPG) with a v/v ratio 75:25 DOPE/DOPG. This ratio produced a net charge similar to the bacterial membrane's net charge. The advantage of the lipids DOPE/DOPG is that their T_m is respectively -16°C and -18°C as opposed to POPE/POPG which could undergo a solid-liquid phase transition at room temperature as POPE has a T_m=25°C.

Chapter 3

Methods

3.1 Materials

Glycerol Monooleate (Rylo MG19Pharma) was obtained from DANISCO DuPont Nutrition Biosciences ApS (Copenhagen, Denmark), Super Refined Oleic Acid (NF-LQ-(MH)) from Croda Inc. (Snaith, United Kingdom), Phytantriol from DSM Nutritional Products Ltd (Wurmisweg, Switzerland), Poloxamer 407 (Lutrol F127) from BASF SE AB (Göteborg, Sweden) and Acetic acid (ACS reagent, purity ≥99,7%) from Sigma-Aldrich (St.Louis, USA). The peptides LL-37 (purity ≥94%) and AP114 (purity ≥99%) were provided by PolyPeptide Group (Limhamn, Sweden). DPK-060 (purity ≥98%) was provided by Bachem AG (Bubendorf, Switzerland). The phospholipids 1,2-dioleoyl-sn-glycero-3-phosphoethanolamine (DOPE) and 1,2-dioleoyl-sn-glycero-3-phospho-(1'-rac-glycerol) (DOPG) were purchased from Avanti Polar Lipids (Alabaster, AL, USA) and were >99% purity. Poly-L-lysine hydrobromide was purchased from Sigma-Aldrich (St.Louis, USA). The water used was purified (TOC ≤ 5 ppb) with milli-Q Integral Water Purification System (Merck Millipore Corporation (Billerica,USA).

3.2 Bulk liquid crystalline phase formulation

The following table summarizes the bulk phase samples formulated. The formulations are based on the phase study in Appendix A.1.

Table 1: *Unloaded bulk phases with relative concentrations.*

Phyt/OA	Lipid/Water	GMO/OA	Lipid/Water
70:30	80:20	80:20	80:20
75:25	80:20	85:15	80:20
80:20	80:20	90:10	80:20
90:10	80:20	95:5	80:20

The gels were prepared by mixing liquid GMO or Phyt together with OA and milli-Q water and centrifuged (MSE Mistral 2000 centrifuge, Tamro Lab AB, Kungens Kurva, Sweden) at 3000 rpm for for 30 minutes. All the samples have mass 2 g and are stored in 7 ml vials. The maximum value uncertainty is ±0,005 g.

The samples from Table 2 were loaded by introducing the peptide into the gel during its formulation in order to guarantee the highest peptide encapsulation possible. The peptide was added in the binary system before the introduction of water, step which brings the formation of the LC gel.
The loaded systems are 80:20 w/w GMO/OA and 90:10 w/w Phyt/OA as they have shown better anisotropicity and structure at the polarized light microscopy.

Table 2: *Loaded bulk phases with relative concentrations.*

Phyt/OA	Lipid/Water	Peptide concentration	Peptide
90:10	80:20	1,0 %	DPK-060
90:10	80:20	1,0 %	LL-37
90:10	80:20	1,0 %	AP114
GMO/OA	Lipid/Water	Peptide concentration	Peptide
80:20	80:20	0,5 %	DPK-060
80:20	80:20	1,0 %	DPK-060
80:20	80:20	1,5 %	DPK-060
GMO/OA	Lipid/Water	Peptide concentration	Peptide
80:20	80:20	0,5 %	AP114
80:20	80:20	1,0 %	AP114
80:20	80:20	1,5 %	AP114
GMO/OA	Lipid/Water	Peptide concentration	Peptide
80:20	80:20	1,0 %	LL-37

The GMO/OA system was chosen as the primary system on which test different peptide concentrations because of issues with the stability of Phyt/OA dispersions (see Section 4.2). Furthermore, phytantriol is not included in the Handbook of Pharmaceutical Excipients[61].
All the gels formulated were stored at room temperature in glass vials wrapped in aluminium foil to avoid any degradation by light.

3.3 Hexagonal phase nanodispersion preparation

All the bulk phase samples in Table 1 and Table 2 were dispersed with a procedure based on the investigations reported in Appendix A.2 and is described below.
The bulk hexagonal phases containing 20% w/w water were added to an acetate buffer solution (5 mM, pH 5.5) containing 1% w/w F127 polymeric stabilizer. The resulting system contains 5% w/w bulk phase dispersed in 95% w/w solution and the sample volume is 10 ml. The polymeric stabilizer and bulk phase concentration choice is based on the research performed by *Lopes et al.*[43].
LC gels were initially pre-dispersed with an T 25 Digital Ultra-Turrax dispersing instrument (IKA-Werke GmbH & Co. KG, Staufen im Breisgau, Germany) for 1 min at 19000 rpm and sonicated with the Vibra-Cell VC 750 Ultrasonic processor (Sonics & Materials Inc., Newtown, USA) for 5 minutes in pulse mode (3 second pulses alternated with 7 second breaks) with amplitude set at 39% with a 6 mm probe. The sonication efficiency is highly dependent on vial shape and volume so identical 21 ml vials were used for all the colloidal systems.
Colloidal samples were stored in 1.5 ml Protein LoBind Tubes (Eppendorf AG, Hamburg, Germany) protected from sunlight with an aluminium foil.

3.4 Characterization of bulk phases and nanodispersions

3.4.1 Visual inspection at polarizer and polarized light microscopy

Polarized light was shone on the bulk samples in order to access their anisotropicity. The morphologies of both the bulk phases and the dispersed phases were characterized by Axio Imager 2 microscope for polarized light (Carl Zeiss AG, Oberkochen, Germany). The magnification

ranged between 10x and 100x.

3.4.2 Particle size determination

Dispersions' hydrodynamic particle size diameter and the Polydispersity Index (PDI) were assessed through a Zetasizer Zen 3600 (Malvern Instruments Ltd, Malvern, United Kingdom). This particle size analyzer makes use of the Dynamic Light Scattering (DLS) technique. A monochromatic laser light irradiates a cuvette containing the sample. Depending on how the sample is diluted, the light passes through the sample more or less unaltered with only a small fraction being scattered by the colloids. The interference of the scattered waves creates a spackle pattern and a goniometer measures the scattering intensities and scattering angles[66]. Three measurements were performed on each sample and the average was computed.
All the dispersions were diluted 10x in milli-Q water and polystyrene 10x10x15 mm disposable cuvettes (Sarstedt AG & Co., Nümbrecht, Germany) were used. The measurements were performed at room temperature.

3.4.3 Zeta potential

Zeta potential measurements were performed with the aid of the Zetasizer Zen 3600 (Malvern Instruments Ltd, Malvern, United Kingdom) at room temperature. The particle-solution interface can be divided into two regions: the stern layer is the inner region where the ions are strongly bound and an outer diffuse region where the atoms are more weakly bound to the particle. The zeta potential is the potential at the boundary between the diffuse region and the dispersant. Within the boundary, atoms in general do not drift away[67].

A laser beam (split into incident and reference beam) irradiates the particles and, when it passes through the center of a particle, a scattered beam is detected at a fixed angle. Then, an electrical field applied to the cell makes the particles move thus giving fluctuations of the intensity of the scattered beam. The zeta potential was calculated from the electrophoretic mobility measured using the Smoluchowski model.
Unless when specified, all dispersions were diluted 20x in milli-Q water and disposable mea-

suring cells were used for the measurements. Three measurements were performed on each sample and the average was computed.

3.4.4 Small Angle X-ray Scattering (SAXS)

SAXS measurements was performed at the beamline 1911-SAXS (1.5 GeV MAX II ring, MAX-LAB laboratory, Lund, Sweden[68]). Bulk samples were placed in between 2 Kapton films in a sample holder and dispersed samples were placed into glass capillaries in a metal holder.
Background scattering was minimized by keeping the detector camera in high vacuum. The detector was set to cover a q-range between 0,1 nm^{-1} and 6 nm^{-1} and its distance from the sample was set to 1456 mm. The radiation wavelength was 0,91 Å. Silver behenate was used as the powder diffraction standard to calibrate the angular scale of the measured intensity. Background measurements were also taken on capillaries filled with milli-Q water and on the sample holder loaded with kapton only in order to filter out any scattering signals coming from those sources.
The measurements were performed on all samples at 22°C and at 37°C for selected samples to test temperature influence. The temperature was controlled using a water bath with a termostat on the sample holder and the samples were let equilibrate at 37°C for 5 min before starting the measurements.

The SAXS spectra images were converted into 1-D scattering plots via the Bli9114 Beamline I911-4 software. The crystalline structures were deduced through x-ray standard techniques by comparing the resulting peak relative positions to the standard ones[38].

The scattering peaks originate from the interplanar spacings d_{hkl} of the crystal structure, where h, k, l are integer numbers called Miller indices which determine a family of planes. Since hexagonal phases are 2-dimensional structures of infinitely long rods, the Miller index $l = 0$. The q value is known as the scattering vector and locates each peak position. It is given by the

following formula[69]:

$$q_{hk} = \frac{2\pi}{d_{hk}} \tag{2}$$

The d_{hk} value is given by the formula:

$$d_{hk} = \left[\frac{4}{3a^2} \left(h^2 + k^2 + hk \right) \right]^{-\frac{1}{2}} \tag{3}$$

By combining the two formulas together, the lattice parameter a corresponding to the distance between two cylinders is given by:

$$a = \frac{4\pi}{\sqrt{3} q_{hk}} \sqrt{h^2 + k^2 + hk} \tag{4}$$

Figure 7 gives a better understanding of the calculated parameters.

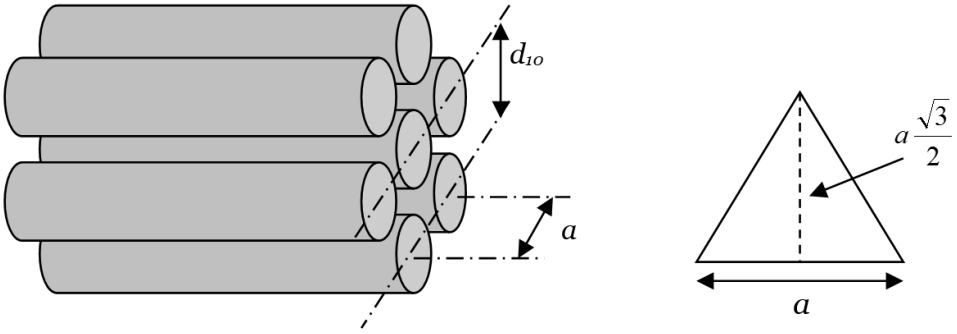

Figure 7: *Lattice parameter a and interplanar spacing* d_{10}.

3.4.5 Cryo-Transmission Electron Microscopy (cryo-TEM)

Dispersed nanoparticle morphologies were inspected through cryo-TEM by Jonny Eriksson (Department of Physical Chemistry, Uppsala University, Uppsala, Sweden).

Obtaining morphology images of amphiphilic compounds in aqueous solutions is a challenging process due to the thermal vibrations of the molecules, the dynamicity and the fragility of the structures especially when subjected to staining and fixation for conventional electron microscopy[49]. Furthermore, regular TEM imaging requires the removal of water which could

result in a loss of internal structure due to the high vacuum. Because of these reasons the sample is subjected to cryogenic temperatures before and during the imaging process, giving the technique the name cryo-TEM.
Sample were prepared in a climate chamber with humidity and temperature control in order to avoid any evaporation. In the chamber, the sample was loaded onto a holey polymer film support on a copper grid and the excess removed by blotting with filter paper. As soon as the sample was situated on the grid, it was submerged into a liquid ethane bath which freezes the sample at -173°C. The liquid ethane bath allowed to freeze the sample almost instantly without forming any crystals. The sample was then transferred into the column of the microscope and then imaged below -160°C.

3.4.6 Ultra Performance Liquid Chromatography (UPLC)

Chromatography is a technique used for the separation of components of a mixture by exploiting the different elution rates of each component from a stationary phase. Before being carried through the stationary phase, the mixture is dissolved in a mobile phase which is liquid in the case of liquid chromatography. The difference in elution rates causes the components to pass through the stationary phase at different speeds. In 2004 UPLC was developed which allowed to achieve significantly higher resolutions, speed, sensitivity while utilizing high pressures and small particle packing[70].
UPLC typically produces an absorbance signal over time. For the purpose of this thesis, UPLC was performed with the purpose of determining the amount of encapsulated peptide. Since the UPLC technique measures the concentration of the filtered sample containing only free peptide in solution (the NPs were filtered out), the bound peptide concentration can be found by subtracting the initial known peptide concentration from the filtered peptide concentration.

UPLC was performed by David Wennman with a Waters Acquity UPLC system with a UV-detector at SP Process Development facilities in Södertälje, Stockholm. The sample preparation is described below and is the same for each of the 3 AMPs.
An Eppendorf tube was filled with a 2,0 ml 0,1% polysorbate 80 solution and stirred. The solvent was let fully evaporate for 15 min in vacuum at 20°C. This procedure allows to coat

the tube with polysorbate 80 and eliminate any water. In a new Eppendorf tube a centrifugal filter unit was placed, 500 μl of 0,1% Lutrol F127 solution added and the system centrifuged (Eppendorf 5415R centrifuge I12174, @RT, 13200 rpm) for 6,5 minutes to separate particles from the dispersion. The (now containing the whole solution) Eppendorf tube was discarded and the filter (now coated with Lutrol F127) was placed in the first tube coated with polysorbate 80. The tube coating helps to significantly lower the amount of peptide bound to the polypropylene.

Since peptides are likely to be absorbed in the filter thus affecting the measurement, solutions of free peptide in acid BSA (Bovine Serum Albumin) solution were filtered at peptide concentrations ranging from 0,47 μg/ml to 106,25 μg/ml employing the previously discussed Eppendorf tubes and centrifugal filter unit. The difference between the initial peptide concentration and the filtered peptide concentration gave the peptide loss which was used as calibration standard.
A test solution with peptide in 5 mM Na-acetate buffer (pH 5,5) was formulated. The AP114 nominal peptide concentration was 52,47 μg/ml, while DPK-060 and LL-37 nominal peptide concentration was 50 μg/ml.

All samples were diluted in 5 mM Na-acetate buffer (pH 5,5) prior to the analysis. Samples with peptide concentration equal or lower than 500 μg/ml were diluted 400 μl in 1600 μl buffer, while sample with peptide concentration 750 μg/ml were diluted 200 μl in 1800 μl. Then, each sample was centrifuged as previously described for 20 minutes. The analysis was performed on 500 μl of each sample.
Each sample was measured twice.

The bounded peptide percentage was obtained through the following formula:

$$\%_{bounded} = \frac{C_{tot} - C_{free}}{C_{tot}} \cdot 100 \tag{5}$$

Where C_{tot} (μg/ml) is the nominal total peptide concentration and C_{free} (μg/ml) is the calculated free peptide concentration in solution after centrifugation.

3.4.7 Liposome preparation

The lipids DOPE and DOPG were purchased dissolved in chloroform and stored in a freezer at -20°C. A chloroform stock solution was prepared of each lipid with 6,5 mM lipid concentration. From the two stock solutions a 2 ml mixture was obtained with a 75:25 DOPE/DOPG v/v ratio in a 10 ml round flask. The chloroform in the mixture was then evaporated with a rotary evaporator (Heidolph Instruments GmbH & Co., Schwabach, Germany) for 40 minutes at 190 rpm, water bath temperature 40°C at a vacuum of ca. 400 mbar. Then, the sample was placed into a vacuum oven (Binder GmbH, Tuttlingen, Germany) overnight at 30°C at ca. 30 mbar. After the process, a visible lipid translucent film was formed on the flask wall.
The film was then rehydrated in Acetate buffer to a 10 mM lipid concentration, vortex mixed for 3 minutes and pipetted into a 10 ml glass vial. The solution was then extruded 15 times through a 100 nm porous membrane and 15 times through a 30 nm membrane. The characterization of liposome size was done with a Zetasizer Zen 3600 and samples were stored at 5°C until further use.

3.4.8 Quartz Crystal Microbalance with Dissipation monitoring (QCM-D)

QCM-D is a technology which enables real-time measurements of molecule adsorption and interaction on a surface[71]. A voltage applied to a quartz crystal causes it to oscillate at its resonance frequency. The measured signals are change in frequency (Δf) and change in damping (ΔD)[72]. Molecules in solution were introduced onto the surface through a pump connected fluidic channels.

The absorbed mass can be calculated through the Sauerbrey relation[73]:

$$\Delta m = \frac{C \cdot \Delta f}{n} \tag{6}$$

Where Δm is the mass of the adhering layer (ng·cm^{-2}), C is a constant (17,7 ng·Hz^{-1}·cm^{-2}) and n is the overtone number.

The change in damping (or dissipation, ΔD) is calculated through the following equation[71]:

$$\Delta D = \frac{E_{dissipated}}{2\pi E_{stored}} \tag{7}$$

Where $E_{dissipated}$ is the energy lost during an oscillation after removing the applied voltage and E_{stored} is the total energy stored in the oscillator.
The change in damping gives information about the rigidity of the adsorbed layer. A high ΔD means that the film is flexible and loose on the surface, while a low ΔD means that the film is rigid and compact[74].

For this thesis, the QCM-D instrument used was Q-Sense E1 equipped with a standard flow module and an accessory chamber, while the sensors used were gold surfaces. All the equipment was manufactured by Biolin Scientific AB (Stockholm, Sweden). The experiment consisted of multiple steps and its main purpose was to create a DOPE/DOPG bilayer onto the gold surface followed by the introduction into the system of a dispersion of hexosomes either unloaded or loaded with peptide.
The mechanisms of adsorption are mainly determined by hydrophobic interactions of the interfaces. An additional poly-L-lysine layer was added in-between the gold surface and the bilayer as described in [19, 16, 21, 22] in order to facilitate its adhesion and to avoid any adsorption of the particles on the gold surface through defects of the bilayer.

The DOPE/DOPG bilayer was formed with a method first developed by *McConnell et al.*[75, 72]. By allowing small unilamellar DOPE and DOPG vesicles come into contact with a clean hydrophilic surface, their rupture is induced thus fusing together and forming a coherent planar bilayer. Once the bilayer formation was assessed, a solution containing 0,1 mg/ml 80:20 GMO/OA hexosomes was introduced and the interaction was studied. For a comparison, measurements with free peptide and loaded particles were also performed.

The solutions were prepared as follows: 0,1 mg/ml poly-L-lysine in milli-Q water, 20 μM DOPE/DOPG in acetate buffer, 0,1 mg/ml 80:20 GMO/OA unloaded hexosomes in acetate buffer, 0,1 mg/ml 80:20 GMO/OA loaded hexosomes in acetate buffer, 1 μg/ml AMP in acetate buffer. All the QCM-D measurements were performed at 37°C and repeated two times.

Chapter 4

Results and Discussion

4.1 Visual inspection and polarized light microscopy

A first control of the samples was performed by visual inspection of physical stability. All bulk phases appear as sticky semitransparent gels to the naked eye and they did not show any signs of phase separation. Dispersed phases appeared as light blue liquid solutions with sporadic formation of bigger agglomerates at the liquid-air interface, a result of a too low sonication time. Dispersed samples were transferred with a pipette to another vial in order to isolate the nanodispersion from agglomerates on the surface.

The morphologies of the bulk phases were investigated with a polarized light microscope. The anisotropicity was confirmed with these images. A λ plate was used to increase the contrast of optical path differences. Figure 8 gives two relevant examples of morphologies observed for the hexagonal phases. No significant difference was found between the peptide loaded and the unloaded samples.

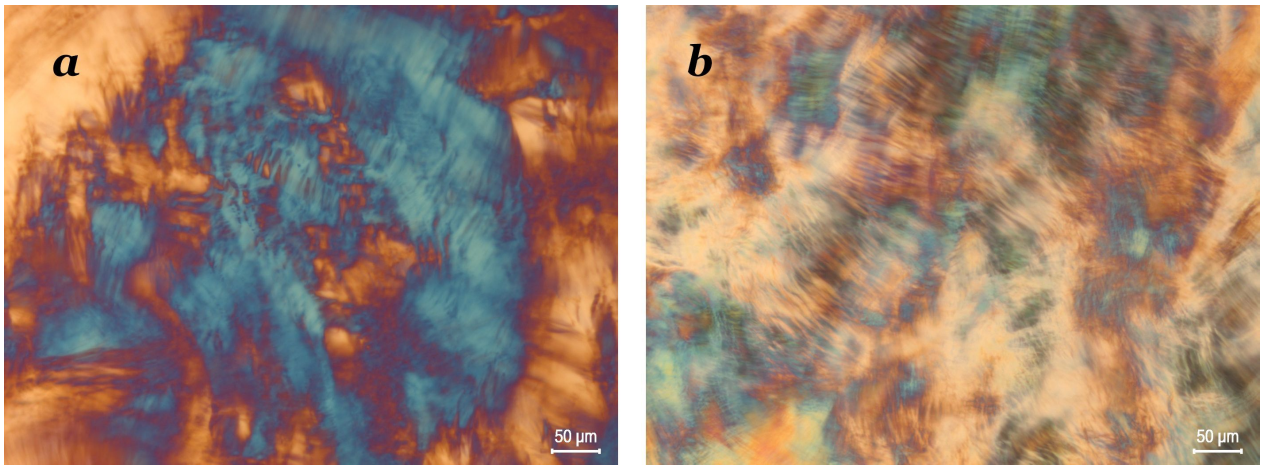

Figure 8: *Polarized light microscopy images of bulk phases at x10 magnification. a)90:10 Phyt/OA loaded with LL-37; b)80:20 GMO/OA loaded with LL-37.*

4.2 Particle size determination and stability

Before performing the size measurements all the GMO/OA dispersions were let equilibrate for 4 days after ultrasonication. From the preliminary ultrasonication tests on the Phyt/OA particles, a growth in size was observed during the first day after ultrasonication. The particle sizes were measured both immediately and 4 days after dispersion.
The data extracted by such measurements are: the size distribution curves and the corresponding volume fraction of each data point, the Z-average which gives a measure of the average size of a particle size distribution, the polydispersity index (PDI) which is a dimensionless value and provides information about the width of the distribution. All data and plots relative to particle size measurements are summarized in Appendix B.2.

No clear trends in size were seen when changing the GMO/OA or Phyt/OA ratio. The biggest influence in particle size seems to be ultrasonication parameters such as sonication time, pulses, magnitude, sample volume and depth of tip immersion and tip position. Even though the parameters were the same for all samples, it was difficult to perform an identical process due to uncertainties such as tip position. Nonetheless, particle sizes were always lower than 350 nm and the distributions were sufficiently narrow for the GMO/OA systems.

Reaching a particle size lower than 500 nm was the goal of the formulation as sizes higher

than such a value would have caused a decrease in particle density leading to particle agglomeration at the surface of the solution.

The Phyt/OA systems were observed to grow in particle size over the first day from sonication and then they stabilized at a value about 60% higher. The F127 stabilizer is probably the reason for the particle growth so efforts were made to vary its concentration in solution but the results were the same.

From Table 3 it appears that the DPK-060, AP114 and LL-37 peptides tend to increase the particle size when loaded into the system, although such an increase is not linear with peptide concentration so it is not possible to obtain any correlation.

Table 3: *Loaded samples' Z-average particle size 4 days after dispersion.*

Phyt/OA	Peptide	Peptide concentration	Particle size [nm]	PDI
90:10	-	-	270,6±2,0	0,285±0,02
90:10	DPK-060	1,0 %	285,83±1,6	0,258±0,005
90:10	LL-370	1,0 %	239,63±1,8	0,242±0,004
90:10	AP114	1,0 %	255,73±1,8	0,239±0,008
GMO/OA	Peptide	Peptide concentration	Particle size [nm]	PDI
80:20	-	-	130,2±1,2	0,307±0,005
80:20	DPK-060	0,5 %	132,53±1,4	0,256±0,018
80:20	DPK-060	1,0 %	123,4±1,0	0,209±0,015
80:20	DPK-060	1,5 %	195,26±0,8	0,174±0,02
80:20	AP114	0,5 %	192,53±1,5	0,181±0,015
80:20	AP114	1,0 %	192,2±0,5	0,178±0,015
80:20	AP114	1,5 %	204,46±5,0	0,146±0,03
80:20	LL-37	1,0 %	179,03±1,2	0,169±0,03

In order to assess the stability of the dispersions over longer periods, size was also evaluated 40 days after preparation for selected samples. Figure 9 shows trends in Z-average particle size growth over time. In Appendix B.2 one can find growth trends of the remaining samples.

The particle size does not seem to increase over 6-7 weeks of storage time, therefore the colloids can be defined as sufficiently stable, especially GMO/OA systems. Although, it must be noted that NPs tend to aggregate in the presence of bigger agglomerates at the surface.

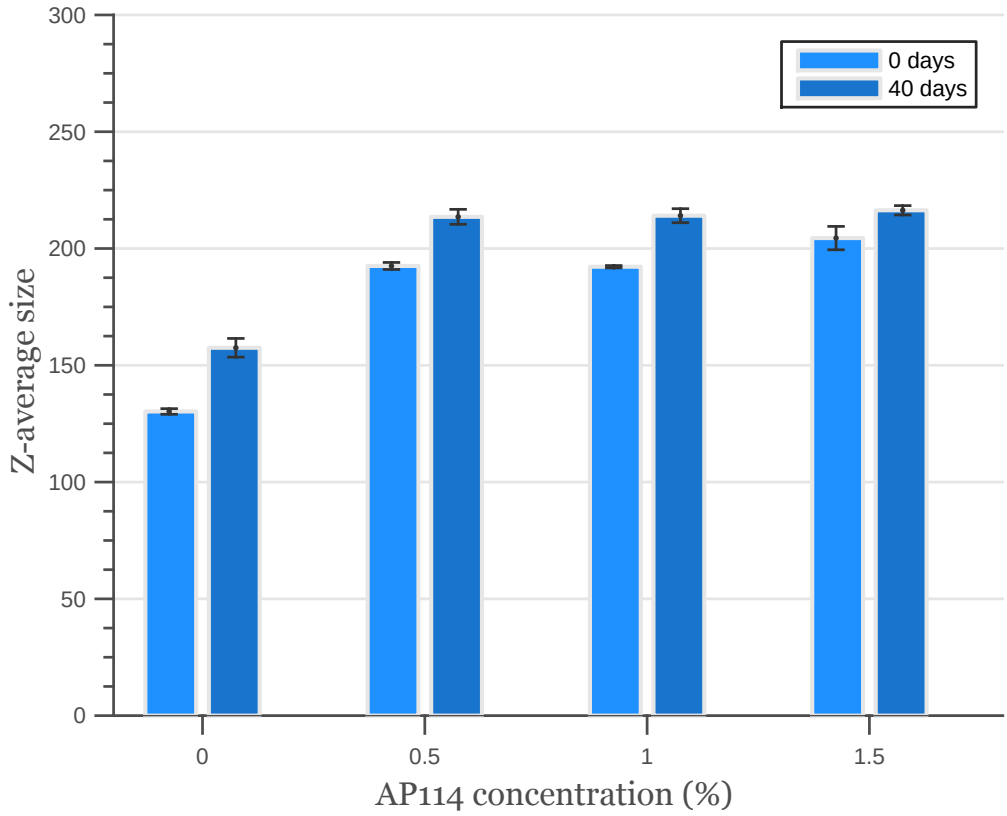

Figure 9: *Size growth trends over a 40 days period of the 80:20 GMO/OA sample loaded with AP114.*

4.3 Zeta potential

The pH of each sample was measured before zeta potential measurements (see Appendix B.4). It appears that the presence of peptides in solution causes the system to become more acidic. The pH change is probably caused by the deprotonation of the carboxyl groups at the n-terminal of the peptide.

The acidity of a solution can modify peptide's net charge thus influencing the zeta potential of the particle the peptide is bounded to. Algorithms[76] can be used for calculating peptide's net charge change with pH. From such calculations it is possible to deduce that in the pH range 4,60 to 5,30 peptide's net charge modifications are unlikely or minor, especially in the case of the peptide DPK-060 (see Appendix B.3). Due to the uncertainty of the other cases, the same measurements were performed on AP114 loaded 80:20 GMO/OA samples diluted in acetate buffer. This solution was less prone to pH changes thus allowing zeta potential measurements to be more reliable.

Once the influence of the pH was confirmed to be limited, zeta potential measurements were performed on all samples. The results are given in Appendix B.4. Unfortunately it is impossible to infer any trend with increasing OA concentration in the LCNPs: the extracted voltages fluctuate around the -30 mV value.

When peptide is introduced in the system the electrostatic behaviour visibly changes. As shown in Figure 10, bound peptides increase the zeta potential in all of the tested dispersions. When the peptide concentration is increased, the zeta potential is increased almost linearly implying that an amount of peptide is located on the surface of the particles.

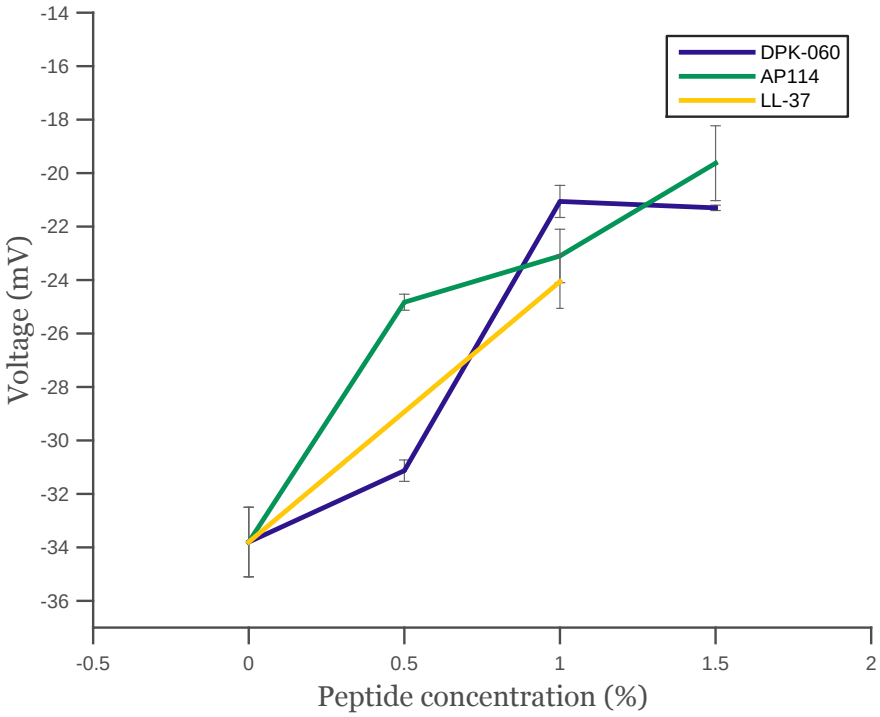

Figure 10: *Zeta potential change of 80:20 GMO/OA samples with peptide concentration variation.*

4.4 Small Angle X-ray Scattering (SAXS)

All bulk and dispersed samples were analyzed by SAXS. Results obtained through this technique are significant because they offer thorough and qualitative information about the generalized internal liquid crystalline structures of each sample. In Appendix B.5 the obtained diffractograms are shown for all samples.

SAXS measurements are presented as plots exhibiting the intensity profiles of scattered curves plotted versus q. By investigating the number of peaks, their width and their relative inter-distance, conclusions about the internal structures of the samples can be deduced. The units of the y axis (Intensity) are arbitrary so it was possible to plot the signals in a semilogarithmic scale and to offset signals coming from similar samples in order to make their comparison easier.

The first observation about the scattering signals is that at a first glance they all exhibit hexagonal patterns. Hexagonal structures show typically peaks with the following spacing ratios:$1:\sqrt{3}:\sqrt{4}:\sqrt{7}:\sqrt{12}$. While the first peak is usually broad and has a very high intensity, the peaks which follow appear narrower and have a significantly lower intensity. The intensities of the 4th and 5th peaks are so low that often do not emerge from the noise signal. For further confirmation those patterns can be easily compared with SAXS measurements performed in some literature papers[43, 77].
Furthermore, the tests performed on unloaded GMO/OA bulk samples with OA concentration variation indicate clearly a phase change on some compositions as shown in Figure 11.

Interestingly, while at 20% OA concentration the phase is hexagonal ($1:\sqrt{3}:\sqrt{4}:\sqrt{7}$ peak spacing ratios), the formation of new peaks is clearly noticeable when the OA concentration in the gel phase is lowered below 10%. Since the additional peaks are presumably originating from a cubic phase (Ia3d), the gels could be constituted by a hexagonal and cubic heterostructure. The presence of two coexisting structures can be explainable in terms of CPP (see Section 2.3). Presumably, in some areas of the gel the amount of OA amphiphiles (with a high CPP) is too small to induce a hexagonal phase formation so in those regions the structure remains cubic. It can be also deduced that OA does not populate homogeneously the whole sample.

Dispersed phase scattering signals have notably lower intensities because these phases are diluted and the gel phase constitutes only 5% of the whole sample. $\sqrt{7}$ peaks and the additional peaks related to cubic phases discussed above are absent hinting that probably the excess water in the dispersion preserves the hexagonal phase.

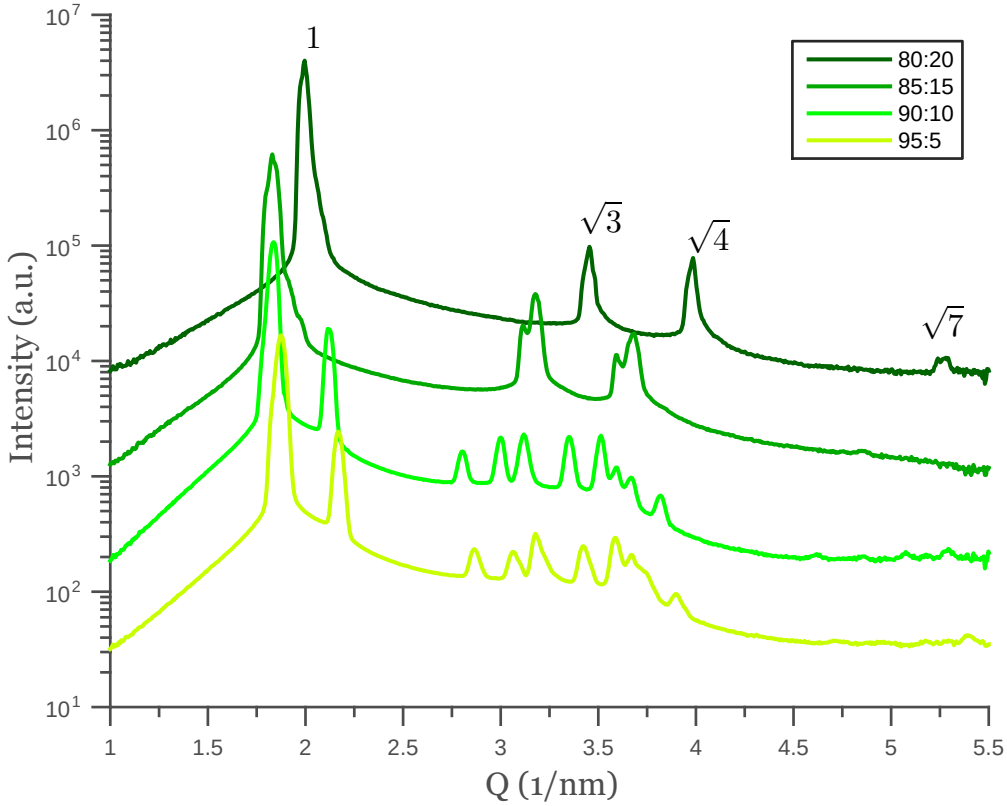

Figure 11: *Unloaded GMO/OA bulk phases with OA concentration variation.*

The goal of decreasing OA concentration trials is to test whether GMO/OA/H_2O ternary phase behaviour studies found in literature could be confirmed[78] with the formulation method employed (a number of process parameters as well as the provenance and purity of the compounds could play a role). It was found that a simple rule of thumb for assuring a hexagonal structure could be to use an OA concentration at least 15-20% in a GMO/H_2O system so the SAXS measurements are consistent with previous phase behaviour studies on these systems.

The phase behaviour of Phyt/OA systems was also reviewed in previous studies, i.e. the research performed by *J.D. Du et al.*[79] in which they locate the hexagonal phase region between 5% and 30% OA concentration at pH 5 of dispersed samples in milli-Q water. Our data from bulk and dispersed phases confirm only partially those observations: the hexagonal phase persists even at OA concentrations as high as 25% with no traces of heterostructures, meaning that the OA concentration could have been further increased.

Both bulk and dispersed liquid crystalline phases preserve their hexagonal structure when AP114, DPK-060 or LL-37 peptides are loaded. Figure 12 gives the AP114 loaded dispersed sample as an example.

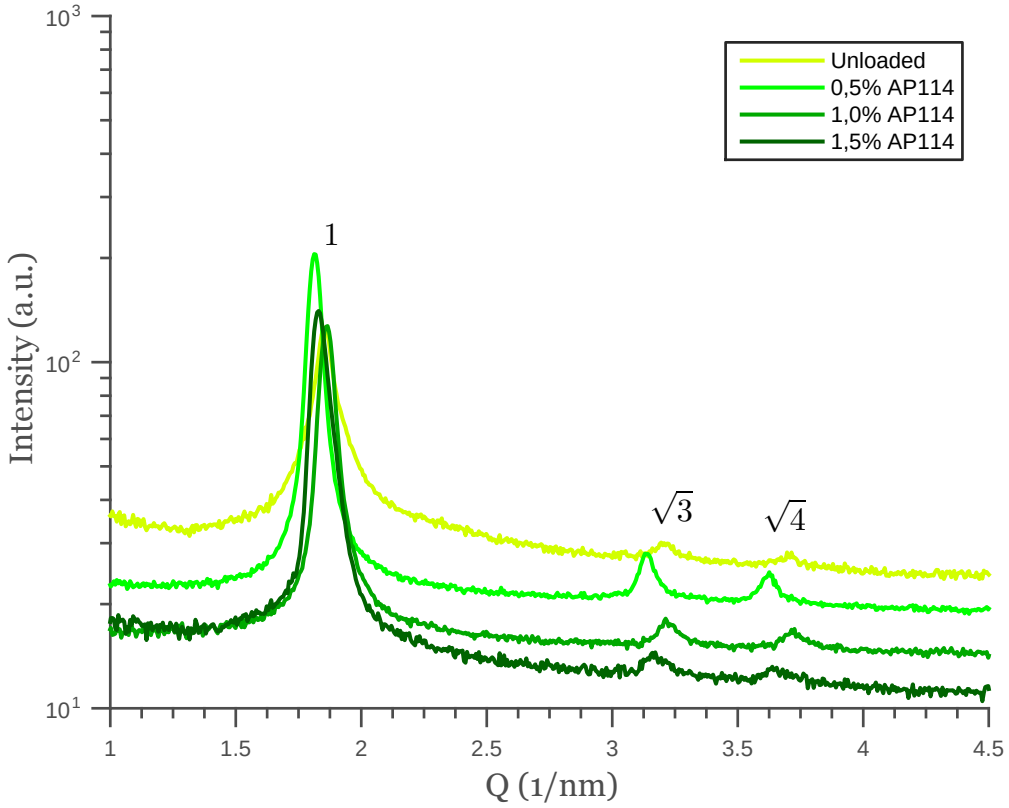

Figure 12: *Loaded 80:20 GMO/OA dispersed phase with AP114 concentration variation.*

In the presence of peptide the lattice parameter tends to increase by 2 to 6 nm for bulk phases and 1 to 2 nm for dispersed phases (see Table 4 and Table 5).

Table 4: *Lattice dimensions with peptide concentration variation in 80:20 GMO/OA bulk samples.*

Peptide	% Peptide	q [nm^{-1}]	Miller index	Peak	d_{hex} [Å]	a_{hex} [Å]	$\overline{a}_{hex}$ [Å]
-	-	1,996	(100)	$\sqrt{1}$	31,48	36,35	36,41
		3,455	(110)	$\sqrt{3}$	18,19	36,37	
		3,974	(200)	$\sqrt{4}$	15,81	36,51	
DPK-060	0,5 %	1,742	(100)	$\sqrt{1}$	36,07	41,65	41,72
		3,01	(110)	$\sqrt{3}$	20,87	41,75	
		3,475	(200)	$\sqrt{4}$	18,08	41,76	
DPK-060	1,0 %	1,724	(100)	$\sqrt{1}$	36,45	42,08	42,07
		2,988	(110)	$\sqrt{3}$	21,03	42,06	
		3,45	(200)	$\sqrt{4}$	18,21	42,06	
DPK-060	1,5 %	1,765	(100)	$\sqrt{1}$	35,6	41,11	41,21
		3,047	(110)	$\sqrt{3}$	20,62	41,24	
		3,514	(200)	$\sqrt{4}$	17,88	41,29	
AP114	0,5 %	1,895	(100)	$\sqrt{1}$	33,16	38,28	38,36
		3,272	(110)	$\sqrt{3}$	19,2	38,4	
		3,779	(200)	$\sqrt{4}$	16,63	38,4	
AP114	1,0 %	1,878	(100)	$\sqrt{1}$	33,45	38,63	38,7
		3,242	(110)	$\sqrt{3}$	19,38	38,76	
		3,75	(200)	$\sqrt{4}$	16,76	38,7	
AP114	1,5 %	1,913	(100)	$\sqrt{1}$	32,84	37,93	37,98
		3,307	(110)	$\sqrt{3}$	19	38	
		3,818	(200)	$\sqrt{4}$	16,46	38	
LL-37	1,0 %	1,795	(100)	$\sqrt{1}$	35	40,42	40,5
		3,101	(110)	$\sqrt{3}$	20,26	40,52	
		3,579	(200)	$\sqrt{4}$	17,56	40,54	

Table 5: *Lattice dimensions with peptide concentration variation in 80:20 GMO/OA dispersed samples.*

Peptide	% Peptide	q [nm^{-1}]	Miller index	Peak	d_{hex} [Å]	a_{hex} [Å]	$\overline{a}_{hex}$ [Å]
-	-	1,854	(100)	$\sqrt{1}$	33,89	39,13	39,15
		3,207	(110)	$\sqrt{3}$	19,59	39,18	
		3,708	(200)	$\sqrt{4}$	16,94	39,13	
DPK-050	0,5 %	1,759	(100)	$\sqrt{1}$	35,72	41,25	41,36
		3,03	(110)	$\sqrt{3}$	20,74	41,47	
		3,508	(200)	$\sqrt{4}$	17,91	41,36	
DPK-060	1,0 %	1,747	(100)	$\sqrt{1}$	35,97	41,53	41,68
		3,012	(110)	$\sqrt{3}$	20,86	41,72	
		3,472	(200)	$\sqrt{4}$	18,1	41,79	
DPK-060	1,5 %	1,724	(100)	$\sqrt{1}$	36,45	42,08	42,2
		2,971	(110)	$\sqrt{3}$	21,15	42,3	
		3,437	(200)	$\sqrt{4}$	18,28	42,22	
AP114	0,5 %	1,813	(100)	$\sqrt{1}$	34,66	40,02	40,08
		3,136	(110)	$\sqrt{3}$	20,04	40,07	
		3,614	(200)	$\sqrt{4}$	17,39	40,15	

AP114	1,0 %	1,866 3,219 3,72	(100) (110) (200)	$\sqrt{1}$ $\sqrt{3}$ $\sqrt{4}$	33,67 19,52 16,89	38,88 39,04 39	38,98
AP114	1,5 %	1,836 3,154 3,638	(100) (110) (200)	$\sqrt{1}$ $\sqrt{3}$ $\sqrt{4}$	34,22 19,92 17,27	39,528 39,84 39,89	39,74
LL-37	1,0 %	1,747 3,012 3,478	(100) (110) (200)	$\sqrt{1}$ $\sqrt{3}$ $\sqrt{4}$	35,97 20,86 18,07	41,529 41,721 41,72	41,657

If one compares the two tables, when the sample is dispersed the lattice parameter a tends to be greater than the bulk phase. Such an increase is probably due to a higher hydration of the liquid crystalline phase in the dispersed case.

Broader peaks and secondary peaks emerge in the DPK-060 case especially at concentrations higher than 1%. The additional peaks could either indicate that the structure is slightly deteriorated or could be originated from liquid crystalline regions which are left peptide-free so not subjected to an increase of lattice parameter.

Selected dispersions were analyzed at 37°C as the stability of the structure must be assessed at conditions typical of topical applications (see Appendix B.5). No significant difference is noticeable and the lattice parameters are similar. It can be concluded that such a temperature change does not affect the structure of the sample.

4.5 Cryo-Transmission Electron Microscopy (Cryo-TEM)

Figure 13 shows representative cryo-TEM images of the GMO/OA systems.

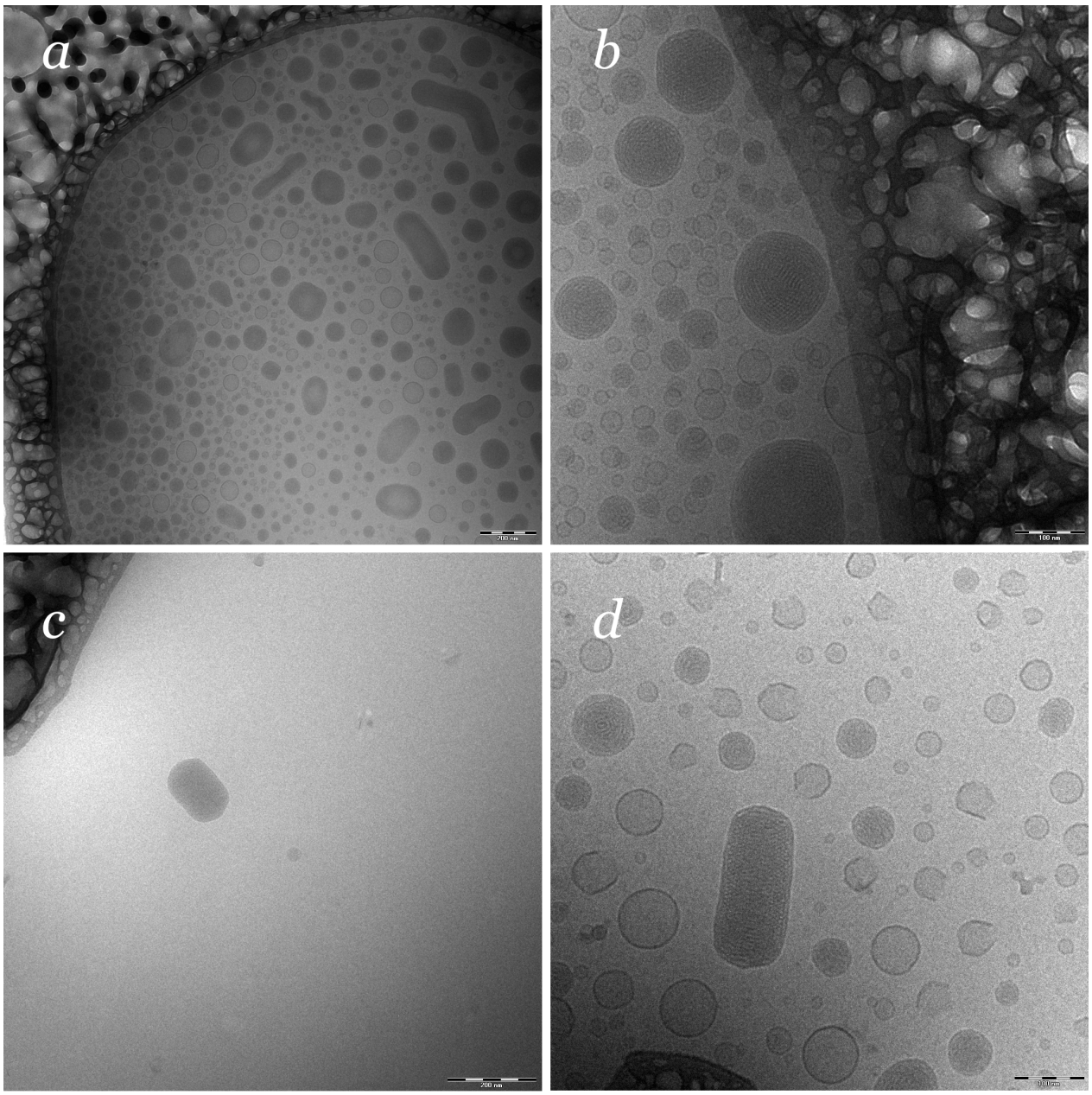

Figure 13: *Cryo-TEM images of 4 dispersed samples: a) unloaded 80:20 GMO/OA; b) unloaded 90:10 GMO/OA; c) 1,0% LL-37 80:20 GMO/OA; d) 1,0% DPK 80:20 GMO/OA.*

From Figure 13 the formation of ordered particles among liposomes can be observed. In this kind of image, ordered structures can be distinguished from the background as they appear

darker while thin and unordered particles appear bright. Since the sample was loaded on a holey polymer film, the whole sample is constrained within such pore which measures between 1 and 6 μm in diameter. The dark region in Figure 13a and Figure 13b corresponds to the thick polymer grid.

The size of the NPs is consistent with size measurements and varies from about 40 nm to 200 nm. The amount of liposomes in solution indicates the efficiency of the formulation method as these vesicles have lower loading efficiency and are unwanted in the system. From Figure 13 it appears that the number of liposomes is in the same order of the number of nanoparticles.
The internal structures of the NPs exhibit spiral patterns similar to rosebuds. By observing cryo-TEM images of similar systems from publications in literature[45, 79, 43], obtaining images of hexagonally shaped nanoparticles with a honeycomb lattice is difficult. The randomness of particle orientation probably limits observations from these 2-D images. Furthermore, growth patterns of the crystalline cylindrical rods are uncertain and the resulting macrostructure could be bipyramidal or irregular so not necessarily rod shaped. Nonetheless, similar spiral patterns were already observed in literature[45, 80] and were credited as typical hexosome shapes.
As in Figure 13 the peptide loaded samples do not display any significant difference from the unloaded samples meaning that the peptide does not disrupt the structure of the particles and is effectively loaded into them.

4.6 Ultra Performance Liquid Chromatography (UPLC)

Drug loading efficiency was measured through UPLC for all peptides DPK-060, AP114 and LL-37. The results are summarized in Table 6 and Table 7.

Table 6: *Loaded Phyt/OA UPLC analysis.*

Peptide	% Peptide	Nominal peptide conc. [μg/ml]	Free peptide conc. [μg/ml]	% Bounded
DPK-060	1,0	500	24,0	≥95
LL-37	1,0	500	21,5	≥96
AP114	1,0	500	413,3	≥17

Table 7: *Loaded GMO/OA UPLC analysis.*

Peptide	% Peptide	Nominal peptide conc. [μg/ml]	Free peptide conc. [μg/ml]	% Bounded
DPK-060	0,5	250	24,0	≥90
DPK-060	1,0	500	24,0	≥95
DPK-060	1,5	750	48,0	≥94
AP114	0,5	250	21,0	≥92
AP114	1,0	500	21,0	≥96
AP114	1,5	750	42,0	≥94
LL-37	1,0	500	39,8	≥92

All the GMO/OA colloidal systems seem to have very high drug loading efficiencies with values between 90% and 96%. Electrostatic interactions have a big influence on measurements via UPLC and such a result is expected due to the highly negative particle charges which were discussed in Section 4.3. Also Phyt/OA systems seem to have overall high efficiencies with values between 92% and 96% except for the AP114 loaded samples which does not seem to overstep the 20% loading efficiency limit.

Two difficulties with the method must be remarked. Such a high peptide adsorption lead to difficulties in the quantification of the efficiency due to the low amount of free peptide in solution (<5 μg/ml) being located outside of the calibration curves thus hindering the accuracy of the measurement. Furthermore, the method was based on the assumption that the peptide concentration was constant in the initial sample. This approximation neglects the presence of any peptide concentration gradient and could lead to some inaccuracies in measurement.

4.7 Quartz Crystal Microbalance with Dissipation monitoring (QCM-D)

Figure 14 depicts the DOPE/DOPG bilayer formation with the QCM-D.
The initial frequency drop of about 260 Hz is caused by the introduction of water into the system, followed by the poly-L-lysine film deposition step which role is to facilitate and provide

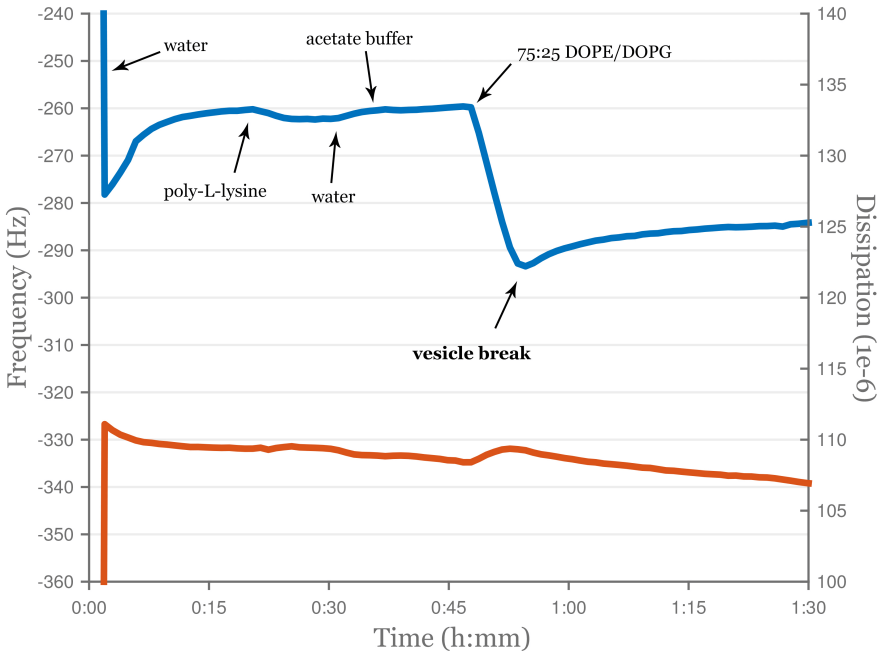

Figure 14: *Resonance frequency drop and dissipation change during poly-l-lysine adsorption and DOPE/DOPG bilayer formation.*

a basis for the bilayer formation. Since the Δf caused by poly-L-lysine is modest, it can be deduced that the film is thin, probably a monolayer.

The DOPE/DOPG vesicle adsorption occurs at around 45 minutes and is followed by the vesicle break and the consequent bilayer formation. The vesicle break kinetics are not known and the process could happen simultaneously upon adsorption, thus not showing the dip in frequency as commonly seen. The behaviour of the vesicles depends on multiple factors such as liposome concentration, flow and liposome composition so it is difficult to predict.

In some previous research[81, 82] the vesicle break step appears to be more distinct than the one observed in these measurements. However, some clues can be found from observing the data. The Δf is 24 Hz which appears to be consistent with these studies and the calculated adsorbed mass is 0,85 mg·m^{-2}. Also, the ΔD appears to slightly increase during the adsorption process (the vesicles situated on the surface are not rigid as they trap water in-between) and then to return to its original value once the bilayer formation is complete. After that, there is no significant increase in ΔD so the structure preserves its rigidity typical of a bilayer.

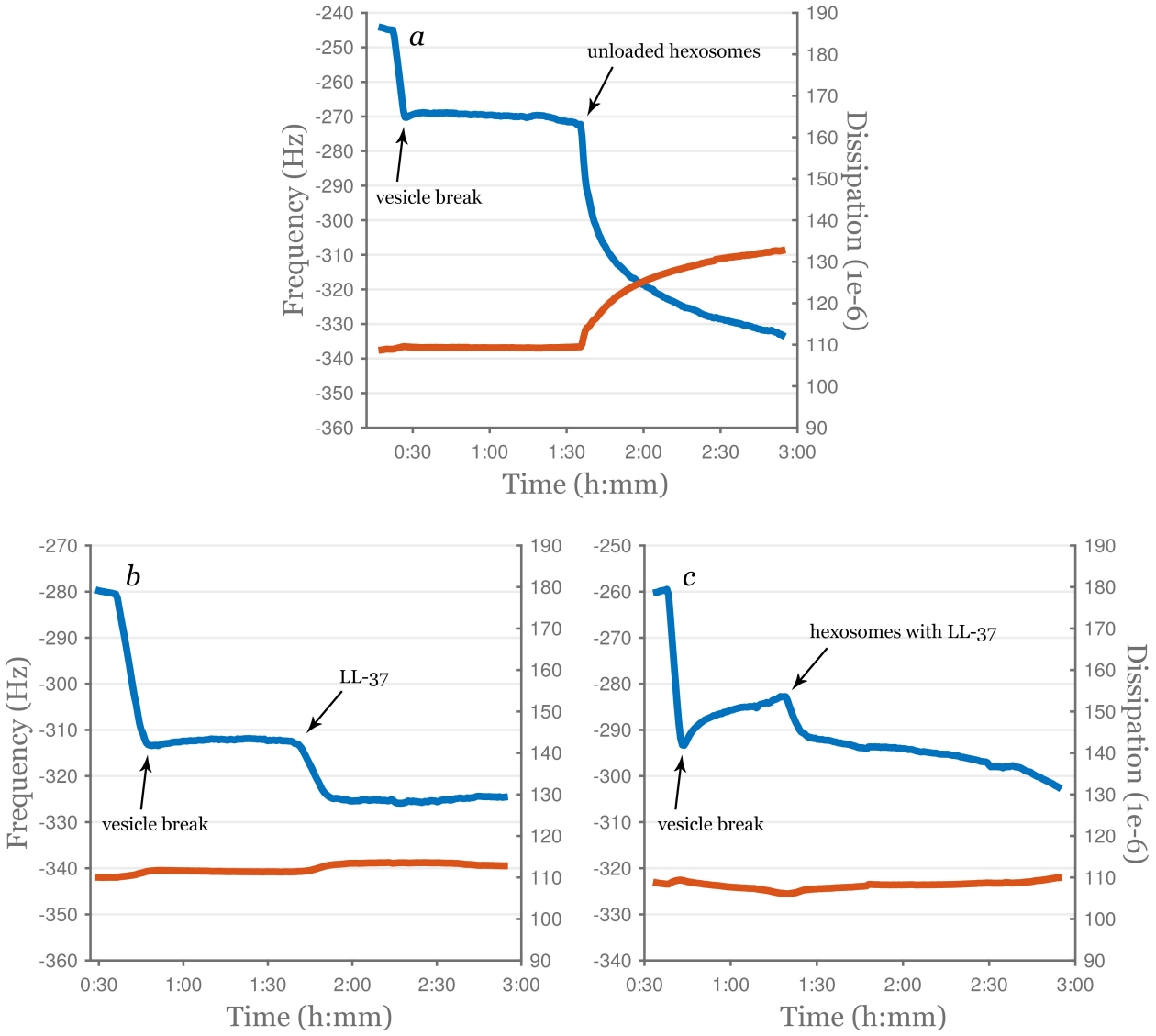

Figure 15: *QCM-D measurements. a)80:20 GMO/OA unloaded hexosomes; b)LL-37 peptide; c) 80:20 GMO/OA hexosomes loaded with LL-37.*

After the bilayer formation step, the adsorption and mechanism of the 3 systems (unloaded 80:20 GMO/OA hexosomes, 80:20 GMO/OA loaded with LL-37 peptide and plain LL-37 peptide) were studied as shown in Figure 15. Unloaded hexosomes (Figure 15a) appear to interact with the membrane very fast and strongly. The adsorption after 1 hour is 2,05 mg·m^{-2} (Δf=59 Hz). The dissipation increases considerably during the adsorption process implying that the particles tend to adhere to the surface and preserve their shape. Water molecules are probably located in-between NPs and increase the dissipation effect. The interaction between the membrane and the hexosomes is probably due to hydrophobic interactions.

When a solution containing plain LL-37 AMP is introduced into the system (Figure 15b), adsorption does not appear to exceed 13 Hz and 0,46 mg·m^{-2} after 1 hour. The slight increase in dissipation probably implies that some damage to the membrane occurs. Also, the mass lost during the process affects the measured Δf which could explain the apparently small adsorption. GMO/OA hexosomes loaded with LL-37 (Figure 15c) appear to maintain the features of the peptide as the Δf after 1 hour is identical to the former case. Although, at longer times hexosomes continue to adsorb due to the membrane allowing more peptide to be targeted on the surface.

Chapter 5

Conclusions and future work

With this thesis a method for hexagonal nanoparticles formulation and peptide encapsulation was proposed. Analysis of the lyotropic phases constituted of GMO/OA and Phyt/OA was performed and the most suitable dispersion method (1 minute blending with an Ultra-Turrax instrument followed by 5 minutes of pulsed ultrasonication) was developed for systems containing peptide.

All the formulations were characterized with a number of techniques. The particle size was determined with DLS and was found to never exceed 300 nm. The colloids appeared to remain stable over long periods of time (40 days) as the particle size did not increase more than 50 nm. Correlations were found between zeta potential and peptide loading. Efforts were made to exclude the influence of pH from such measurements. It was found that an increasing concentration of peptide in the system tends to shift zeta potentials to less negative values.
SAXS diffractograms confirmed that both bulk and dispersed samples have hexagonal structures and peptides did not appear to change the structure. The morphologies of relevant samples were investigated with cryo-TEM. Even though it is difficult to locate any clear hexagonal structures, the observations are consistent with studies on hexagonal phases in literature.
Peptide loading efficiency was assessed with UPLC and was determined to be more than 90% in most of the cases.

The interaction of the hexosome dispersions was studied with QCM-D. Unloaded hexo-

somes appear to have a very high affinity with the model membranes as their adsorption rate is very high. Furthermore, hexosomes do not compromise the effectiveness of the LL-37 peptide as the behaviour of the LL-37 loaded hexosome system is similar to the system with plain peptide.

In the future additional tests could be performed on these systems.
The dispersion method might be investigated further as the current one leads to some drawbacks. A large amount of liposomes was observed in the dispersion as a result of the ultrasonication procedure. Additionally, the sonicating tip is likely to release titanium in solution. A common method for removing titanium particles is to centrifuge the sample thus allowing these heavy particles to deposit on the bottom of the vial and afterwards drain out the sample with a pipette. This step could be useful for securing low contamination of the sample.

QCM-D interfacial sensing of systems interacting with a bacterial membrane can be paired with ellipsometry measurements for an increased understanding of the phenomena involved in the process. QCM-D gives information on the absorbed mass and change in damping so it can be very useful to measure the thickness of the layers as well. Surface plasmon resonance (SPR) is a technique which measures adsorption on a surface (typically gold or silver) with a different mechanism than QCM-D so it would be useful to compare the data of these two measurements. Membrane leakage studies could also give more information on the membrane disruption.

Moreover, further investigations must be performed including assessment of the antimicrobial effect, skin irritation tests and toxicity tests.

Acknowledgments

First of all I wish to express my most sincere gratitude to my supervisor, Lukas Boge for being a great guide and teacher throughout the project, for supporting me in all the research connected to this work and for involving me in amazing experiments such as SAXS and cryo-TEM. If it wasn´t for you, probably I´d still be trying to figure out how to pipette GMO out of the jar.

I am really grateful to Helena Bysell, the FORMAMP project coordinator, for giving me the opportunity of being part of this project and for giving me precious advices during my work. I would also like to thank Lovisa Ringstad for helping me with everything related to peptides and Jesper Hedin for teaching me to run the QCM-D.

I would also like to thank Prof. Mark Rutland for the academic support.

A special thank you goes to Jonny Eriksson and Katarina Edwards for assisting me with the cryo-TEM imaging, to Erich Schuster and Ana Labrador for helping me with SAXS measurements and to David Wennman for performing the UPLC measurements.
I would also like to thank the whole staff at the SP Chemistry, Materials and Surfaces department for being so supportive and for helping me with all he daily problems I had in the lab!

The research leading to these results has received funding from the European Union Seventh Framework Programme (FP7/2007-2013) under grant agreement n° 604182 through the FORMAMP project

Bibliography

[1] R. I. Aminov, "A brief history of the antibiotic era: lessons learned and challenges for the future," *Frontiers in Microbiology, Vol 1 (2010)*, 2010.

[2] S. Duckett, "Ernest duchesne and the concept of fungal antibiotic therapy," *The Lancet*, vol. 354, no. 9195, pp. 2068–2071, 1999.

[3] M. Mike, "Antibiotics," *Nature*, vol. 509, no. 7498, p. S1, 2014.

[4] World Health Organization, *Antimicrobial resistance: global report on surveillance*. 2014.

[5] D. Skinner, "Significance of bacteremia caused by staphylococcus aureus," *Archives of Internal Medicine*, vol. 68, no. 5, p. 851, 1941.

[6] F. D. Lowy, "Antimicrobial resistance: the example of staphylococcus aureus," *The Journal of clinical investigation*, vol. 111, no. 9, p. 1265, 2003.

[7] R. Laxminarayan and A. Malani, "Extending the cure," report, 2007.

[8] M. R. Yeaman and N. Y. Yount, "Mechanisms of antimicrobial peptide action and resistance," *Pharmacological reviews*, vol. 55, no. 1, p. 27, 2003.

[9] N. Sewald, *Peptides: Chemistry and Biology*. 2002.

[10] "The Antimicrobial Peptide Database." http://aps.unmc.edu/AP/main.php. Accessed: 2015-06-03.

[11] A. R. Koczulla and R. Bals, "Antimicrobial peptides: current status and therapeutic potential," *Drugs*, vol. 63, no. 4, p. 389, 2003.

[12] M. N. Melo, R. Ferre, and M. A. R. B. Castanho, "Antimicrobial peptides: linking partition, activity and high membrane-bound concentrations," *Nature reviews. Microbiology*, vol. 7, no. 3, p. 245, 2009.

[13] M. M. Welling, A. Paulusma-Annema, H. S. Balter, E. K. J. Pauwels, and P. H. Nibbering, "Technetium-99m labelled antimicrobial peptides discriminate between bacterial infections and sterile inflammations," *Eur. J. Nucl. Med.*, vol. 27, no. 3, pp. 292–301, 2000.

[14] M. Pasupuleti, A. Schmidtchen, and M. Malmsten, "Antimicrobial peptides: key components of the innate immune system," *Critical Reviews in Biotechnology*, vol. 32, no. 2, pp. 143–171, 2012.

[15] L. Ringstad, "Interaction between antimicrobial peptides and phospholipid membranes effects of peptide length and composition," 2009.

[16] L. Ringstad, L. Kacprzyk, A. Schmidtchen, and M. Malmsten, "Effects of topology, length, and charge on the activity of a kininogen-derived peptide on lipid membranes and bacteria," *BBA - Biomembranes*, vol. 1768, no. 3, pp. 715–727, 2007.

[17] M. Malmsten, "Antimicrobial peptides," *Uppsala Journal of Medical Sciences, 2014, Vol.119(2), p.199-204*, vol. 119, no. 2, pp. 199–204, 2014.

[18] M. Pasupuleti, A. Schmidtchen, and M. Malmsten, "Antimicrobial peptides: key components of the innate immune system," *Critical Reviews in Biotechnology*, vol. 32, no. 2, pp. 143–171, 2012.

[19] L. Ringstad, A. Schmidtchen, and M. Malmsten, "Effect of peptide length on the interaction between consensus peptides and dopc/dopa bilayers," *Langmuir : the ACS journal of surfaces and colloids*, vol. 22, no. 11, p. 5042, 2006.

[20] B. Deslouches, S. M. Phadke, V. Lazarevic, M. Cascio, K. Islam, R. C. Montelaro, and T. A. Mietzner, "De novo generation of cationic antimicrobial peptides: Influence of length and tryptophan substitution on antimicrobial activity," *Antimicrobial Agents and Chemotherapy*, vol. 49, no. 1, p. 316, 2005.

[21] L. Ringstad, E. Andersson Nordahl, A. Schmidtchen, and M. Malmsten, "Composition effect on peptide interaction with lipids and bacteria: Variants of c3a peptide cny21," *Biophysical Journal*, vol. 92, no. 1, pp. 87–98, 2007.

[22] L. Ringstad, E. Protopapa, B. Lindholm-Sethson, A. Schmidtchen, A. Nelson, and M. Malmsten, "An electrochemical study into the interaction between complement-derived peptides and dopc mono- and bilayers," *Langmuir*, vol. 24, no. 1, pp. 208–216, 2008.

[23] M. Zasloff, "Antimicrobial peptides of multicellular organisms," *Nature*, vol. 415, no. 6870, p. 389, 2002.

[24] Y. Shai, "Mode of action of membrane active antimicrobial peptides," 2002.

[25] D. Sengupta, H. Leontiadou, A. E. Mark, and S.-J. Marrink, "Toroidal pores formed by antimicrobial peptides show significant disorder," *BBA - Biomembranes*, vol. 1778, no. 10, pp. 2308–2317, 2008.

[26] G. Ehrenstein and H. Lecar, "Electrically gated ionic channels in lipid bilayers," *Quart. Rev. Biophys.*, vol. 10, no. 1, pp. 1–34, 1977.

[27] D. I. Fernandez, A. P. Le Brun, T. C. Whitwell, M.-a. Sani, M. James, and F. Separovic, "The antimicrobial peptide aurein 1.2 disrupts model membranes via the carpet mechanism," *Phys. Chem. Chem. Phys.*, vol. 14, no. 45, pp. 15739–15751, 2012.

[28] S. Thennarasu, A. Tan, R. Penumatchu, C. E. Shelburne, D. L. Heyl, and A. Ramamoorthy, "Antimicrobial and membrane disrupting activities of a peptide derived from the human cathelicidin antimicrobial peptide ll37," *Biophysical Journal*, vol. 98, no. 2, pp. 248–257, 2010.

[29] U. H. N. Dürr, U. S. Sudheendra, and A. Ramamoorthy, "Ll-37, the only human member of the cathelicidin family of antimicrobial peptides," *Biochimica et biophysica acta*, vol. 1758, no. 9, p. 1408, 2006.

[30] N. Mookherjee and R. Hancock, "Cationic host defence peptides: Innate immune regulatory peptides as a novel approach for treating infections," *Cell. Mol. Life Sci.*, vol. 64, no. 7, pp. 922–933, 2007.

[31] Pergamum AB, "Pergamum initiates phase ii trial with dpk-060 in outer ear infections." http://www.pergamum.com/blog/pergamum-initiates-phase-ii-trial-with-dpk-060-in-outer-ear-infections/, 2012. Accessed: 2015-05-20.

[32] Karolinska Development AB. http://www.karolinskadevelopment.com/en/portfolio/infections-and-wound-healing/dpk-060/. Accessed: 2015-05-20.

[33] Pergamum AB, DermaGen AB, "A study of dpk-060 to investigate clinical safety and efficacy in patients with acute external otitis." https://clinicaltrials.gov/ct2/show/NCT01447017, 2013. Accessed: 2015-05-20.

[34] H. M. Per, L. F. Rikke, M. S. Kirk, T. H. Mogens, P. S. Carsten, L. Svend, R. Dorotea, B. Steen, C. Bjarke, M. Leonardo De, T. Olivier, Y. Debbie, G. E.-J. Signe, V. S. Marianne, E. C. Bjørn, K. Søren, F.-M. Niels, I. L. Robert, Z. Michael, and K. Hans-Henrik, "Plectasin is a peptide antibiotic with therapeutic potential from a saprophytic fungus," *Nature*, vol. 437, no. 7061, p. 975, 2005.

[35] T. Schneider, T. Kruse, R. Wimmer, I. Wiedemann, V. Sass, U. Pag, A. Jansen, A. K. Nielsen, P. H. Mygind, D. S. Raventós, S. Neve, B. Ravn, A. M. J. J. Bonvin, L. D. Maria, A. S. Andersen, L. K. Gammelgaard, H. G. Sahl, and H. H. Kristensen, "Plectasin, a fungal defensin, targets the bacterial cell wall precursor lipid ii," *Science*, vol. 328, pp. 1168–8075, 2010.

[36] G. G. Perron, M. Zasloff, and G. Bell, "Experimental evolution of resistance to an antimicrobial peptide," *Proceedings. Biological sciences / The Royal Society*, vol. 273, no. 1583, p. 251, 2006.

[37] J. L. Anaya-Lopez, J. E. Lopez-Meza, and A. Ochoa-Zarzosa, "Bacterial resistance to cationic antimicrobial peptides," *Critical Reviews in Microbiology, 2013, Vol.39(2)*, vol. 39, no. 2, pp. 180–195, 2013.

[38] S. T. Hyde, *Handbook of applied surface and colloid chemistry. Vol. 2, Chapter 16.* Chichester: Chichester : Wiley, 2002.

[39] S. Milak and A. Zimmer, "Glycerol monooleate liquid crystalline phases used in drug delivery systems," *International Journal of Pharmaceutics*, vol. 478, no. 2, pp. 569–587, 2015.

[40] P. J. Collings, *Introduction to Liquid Crystals: Chemistry and Physics*. Hoboken: Hoboken : Taylor and Francis, 1997.

[41] J. P. F. Lagerwall and G. Scalia, "A new era for liquid crystal research: Applications of liquid crystals in soft matter nano-, bio- and microtechnology," *Current Applied Physics*, vol. 12, no. 6, pp. 1387–1412, 2012.

[42] A. Lancelot, T. Sierra, and J. L. Serrano, "Nanostructured liquid-crystalline particles for drug delivery," *Expert Opinion on Drug Delivery, 2014, Vol.11(4)*, vol. 11, no. 4, pp. 547–564, 2014.

[43] L. Lopes, D. Ferreira, D. Paula, M. Garcia, J. Thomazini, M. Fantini, and M. Bentley, "Reverse hexagonal phase nanodispersion of monoolein and oleic acid for topical delivery of peptides: in vitro and in vivo skin penetration of cyclosporin a," *An Official Journal of the American Association of Pharmaceutical Scientists*, vol. 23, no. 6, pp. 1332–1342, 2006.

[44] G. H. Brown and J. J. Wolken, *Liquid Crystals and Biological Structures*. United States: Academic Press, 1979.

[45] X. Mulet, B. J. Boyd, and C. J. Drummond, "Advances in drug delivery and medical imaging using colloidal lyotropic liquid crystalline dispersions," *Journal of Colloid And Interface Science*, 2012.

[46] K. Holmberg, *Surfactants and Polymers in Aqueous Solution*. 2002.

[47] R. Hirlekar, S. Jain, M. Patel, H. Garse, and V. Kadam, "Hexosomes: A novel drug delivery system," *Current Drug Delivery*, vol. 7, no. 1, pp. 28–35, 2010.

[48] Y. D. Dong, I. Larson, T. Hanley, and B. J. Boyd, "Bulk and dispersed aqueous phase behavior of phytantriol: effect of vitamin e acetate and f127 polymer on liquid crystal nanostructure," *Langmuir : the ACS journal of surfaces and colloids*, vol. 22, no. 23, p. 9512, 2006.

[49] M. Almgren, K. Edwards, and G. Karlsson, "Cryo transmission electron microscopy of liposomes and related structures," *Colloids and Surfaces A: Physicochemical and Engineering Aspects*, vol. 174, no. 1, pp. 3–21, 2000.

[50] F. Muller, A. Salonen, and O. Glatter, "Phase behavior of phytantriol/water bicontinuous cubic pn3m cubosomes stabilized by laponite disc-like particles," *Journal of Colloid And Interface Science*, vol. 342, no. 2, pp. 392–398, 2010.

[51] H. Chung, J. Kim, J. Y. Um, I. C. Kwon, and S. Y. Jeong, "Self-assembled "nanocubicle" as a carrier for peroral insulin delivery," *Clinical and Experimental Diabetes and Metabolism*, vol. 45, no. 3, pp. 448–451, 2002.

[52] S. B. Rizwan, D. Assmus, A. Boehnke, T. Hanley, B. J. Boyd, T. Rades, and S. Hook, "Preparation of phytantriol cubosomes by solvent precursor dilution for the delivery of protein vaccines," *European Journal of Pharmaceutics and Biopharmaceutics*, vol. 79, no. 1, pp. 15–22, 2011.

[53] S. B. Rizwan, T. Hanley, B. J. Boyd, T. Rades, and S. Hook, "Liquid crystalline systems of phytantriol and glyceryl monooleate containing a hydrophilic protein: Characterisation, swelling and release kinetics," *Journal of Pharmaceutical Sciences*, vol. 98, no. 11, pp. 4191–4204, 2009.

[54] S. Gordon, K. Young, R. Wilson, S. Rizwan, R. Kemp, T. Rades, and S. Hook, "Chitosan hydrogels containing liposomes and cubosomes as particulate sustained release vaccine delivery systems," *Journal of Liposome Research, 2012, Vol.22(3), p.193-204*, vol. 22, no. 3, pp. 193–204, 2012.

[55] T. Rattanapak, K. Young, T. Rades, and S. Hook, "Comparative study of liposomes, transfersomes, ethosomes and cubosomes for transcutaneous immunisation: characterisation and in vitro skin penetration," *Journal of Pharmacy and Pharmacology*, vol. 64, no. 11, pp. 1560–1569, 2012.

[56] C. Cervin, P. Vandoolaeghe, C. Nistor, F. Tiberg, and M. Johnsson, "A combined in vitro and in vivo study on the interactions between somatostatin and lipid-based liquid crystalline drug carriers and bilayers," *European Journal of Pharmaceutical Sciences*, vol. 36, no. 4, pp. 377–385, 2009.

[57] J. Lai, Y. Lu, Z. Yin, F. Hu, and W. Wu, "Pharmacokinetics and enhanced oral bioavailability in beagle dogs of cyclosporine a encapsulated in glyceryl monooleate/poloxamer 407 cubic nanoparticles," *International journal of nanomedicine*, vol. 5, p. 13, 2010.

[58] A. A. Stromstedt, M. Pasupuleti, A. Schmidtchen, and M. Malmsten, "Evaluation of strategies for improving proteolytic resistance of antimicrobial peptides by using variants of efk17, an internal segment of ll-37," *Antimicrobial Agents and Chemotherapy*, vol. 53, no. 2, p. 593, 2009.

[59] J. Lai, J. Chen, Y. Lu, J. Sun, F. Hu, Z. Yin, and W. Wu, "Glyceryl monooleate/poloxamer 407 cubic nanoparticles as oral drug delivery systems: I. in vitro evaluation and enhanced oral bioavailability of the poorly water-soluble drug simvastatin," *AAPS PharmSciTech*, vol. 10, no. 3, pp. 960–966, 2009.

[60] B. J. Boyd, S.-M. Khoo, D. V. Whittaker, G. Davey, and C. J. H. Porter, "A lipid-based liquid crystalline matrix that provides sustained release and enhanced oral bioavailability for a model poorly water soluble drug in rats," *International Journal of Pharmaceutics*, vol. 340, no. 1, pp. 52–60, 2007.

[61] *Handbook of Pharmaceutical Excipients*. Pharmaceutical Press, 2009.

[62] Personal Care Products Council, "Phytantriol." http://cosmeticsinfo.org/ingredient/ phytantriol, 2015. Accessed: 2015-05-20.

[63] J. Barauskas and T. Landh, "Phase behavior of the phytantriol/water system," *Langmuir*, vol. 19, no. 23, pp. 9562–9565, 2003.

[64] P. Yeagle, *The membranes of cells*. Orlando: Academic Press, 1987.

[65] J. T. J. Cheng, J. D. Hale, M. Elliott, R. E. W. Hancock, and S. K. Straus, "The importance of bacterial membrane composition in the structure and function of aurein 2.2 and selected variants," *BBA - Biomembranes*, vol. 1808, no. 3, pp. 622–633, 2010.

[66] D. W. Bruce, D. Hare, and R. I. Walton, *Multi Length-Scale Characterisation: Inorganic Materials Series*. Wiley, 2013.

[67] Malvern Instruments Ltd, "Zeta potential: An introduction in 30 minutes - technical note." http://www3.nd.edu/ rroeder/ame60647/slides/zeta.pdf. Accessed: 2015-05-20.

[68] MAX IV Laboratory, "Home i911-saxs." https://www.maxlab.lu.se/node/727. Accessed: 2015-05-20.

[69] M. Kjellin, "Structure-property relationships of surfactants at interfaces and polyelectrolyte-surfactant aggregates," 2002.

[70] Waters Corporation, "Beginner's Guide to UPLC." http://www.waters.com/waters/en_US /Primers/nav.htm?cid=10048920. Accessed: 2015-05-20.

[71] Biolin Scientific AB, "Quartz Crystal Microbalance with Dissipation (QCM-D)." http://www.biolinscientific.com/zafepress.php?url=/pdf/Q-Sense/Technology Accessed: 2015-06-03.

[72] E. Reimhult, M. Zäch, F. Höök, and B. Kasemo, "A multitechnique study of liposome adsorption on au and lipid bilayer formation on sio2," *Langmuir : the ACS journal of surfaces and colloids*, vol. 22, no. 7, p. 3313, 2006.

[73] Biolin Scientific AB, "QCM-D: Dissipation Monitoring Enables Accurate Analysis of Soft Materials." http://www.biolinscientific.com/q-sense/technologies/?card=QT1. Accessed: 2015-06-03.

[74] G. McCubbin, S. Praporski, S. Piantavigna, D. Knappe, R. Hoffmann, J. Bowie, F. Separovic, and L. Martin, "Qcm-d fingerprinting of membrane-active peptides," *with Biophysics Letters*, vol. 40, no. 4, pp. 437–446, 2011.

[75] H. M. McConnell, T. H. Watts, R. M. Weis, and A. A. Brian, "Supported planar membranes in studies of cell-cell recognition in the immune system," *Biochimica et biophysica acta*, vol. 864, no. 1, p. 95, 1986.

[76] Bio-Synthesis inc. http://www.biosyn.com/PeptidePropertyCalculator/PeptideProperty Calculator.aspx. Accessed: 2015-05-30.

[77] C. Nilsson, B. Barrios-Lopez, A. Kallinen, P. Laurinmäki, S. J. Butcher, M. Raki, J. Weisell, K. Bergström, S. W. Larsen, J. Østergaard, C. Larsen, A. Urtti, A. J. Airaksinen, and A. Yaghmur, "Spect/ct imaging of radiolabeled cubosomes and hexosomes for potential theranostic applications," *Biomaterials*, vol. 34, no. 33, pp. 8491–8503, 2013.

[78] J. Barauskas, M. Johnsson, F. Joabsson, and F. Tiberg, "Cubic phase nanoparticles (cubosome): Principles for controlling size, structure, and stability," *Langmuir*, vol. 21, no. 6, pp. 2569–2577, 2005.

[79] J. D. Du, Q. Liu, S. Salentinig, T.-H. Nguyen, and B. J. Boyd, "A novel approach to enhance the mucoadhesion of lipid drug nanocarriers for improved drug delivery to the buccal mucosa," *International Journal of Pharmaceutics*, vol. 471, no. 1-2, pp. 358–365, 2014.

[80] C. Fong, T. Le, and C. J. Drummond, "Lyotropic liquid crystal engineering–ordered nanostructured small molecule amphiphile self-assembly materials by design," *Chemical Society Reviews*, vol. 41, no. 3, p. 1297, 2012.

[81] H.-h. Shen, P. G. Hartley, M. James, A. Nelson, H. Defendi, and K. M. McLean, "The interaction of cubosomes with supported phospholipid bilayers using neutron reflectometry and qcm-d," *Soft Matter*, vol. 7, no. 18, pp. 8041–8049, 2011.

[82] Biolin Scientific AB, "Lipid Bilayer Formation Using the Q-Sense Open Module." http://www.biolinscientific.com/zafepress.php?url=/pdf/Q-Sense/Technology Accessed: 2015-06-08.

[83] N. Swarnakar, V. Jain, V. Dubey, D. Mishra, and N. K. Jain, "Enhanced oromucosal delivery of progesterone via hexosomes," *An Official Journal of the American Association of Pharmaceutical Scientists*, vol. 24, no. 12, pp. 2223–2230, 2007.

Appendix A

Preliminary investigations

A.1 Initial phase study

As already introduced, the two chosen systems were GMO/OA and Phyt/OA.
Firstly only unloaded gels were formulated. The purpose of this investigation was to determine which GMO/OA w/w ratios and Phyt/OA w/w ratios could potentially give an anisotropic and hexagonal structure. Particular attention was also given to the amount of water to add to the mixtures in order to obtain the desired gels.

A preliminary choice of the ratios was evaluated basing on previous investigations in literature. In particular, *Lopes et al.* research[43] seemed to be a good starting point for the GMO/OA system: GMO/OA hexagonal gels were formulated successfully by using a 80:20 w/w ratio with a lipid weight concentration being 90% in water. As for the Phyt/OA system, the phase diagram provided by *J.D. Du et al.*[79] and the formulation method produced by *Nilsson et al.*[77] gave sufficient insight on the behaviour of the system.
As a result, the following gels were preliminarily evaluated:

- 80:20 w/w GMO/OA in 80:20, 90:10 and 95:5 w/w lipid/water
- 60:40 w/w GMO/OA in 80:20, 90:10 and 95:5 w/w lipid/water
- 90:10 w/w GMO/OA in 80:20, 90:10 and 95:5 w/w lipid/water

- 90:10 w/w Phyt/water
- 80:20 w/w Phyt/water

Please note that the last two gels have been added in order to test the influence of OA in the Phyt gel structure.

The gel preparation process is straightforward. GMO was melted at 45°C and gels were obtained simply by stirring the two compounds together with a spatula. The desired amount of water was added with a pipette and then stirred again until a homogeneous gel was formed. During the water addition step the viscosity of the system increases significantly: the viscous liquid takes the shape of a gel. The gel was centrifuged (3000 RPM, @RT) for 30 minutes. This sticky gel exhibits a white translucent color.
The anisotropicity of the samples was then assessed both by visual inspection and by polarized light microscopy.

- Visual inspection with polarized light: the anisotropicity of the samples could be instantly assessed by shining light on the sample while interposing two polarizing filters in between the observer, the sample and the light source. The 80:20 w/w GMO/OA system with 20% of water, the 90:10 w/w Phyt/OA with 20% of water and the 90:10 w/w Phyt/water systems showed to be the most anisotropic.
- Polarized light microscopy: it was performed in order to distinguish lamellar phases from other anisotropic (possibly hexagonal) phases. Lamellar phases show characteristic spherulite patterns (maltese crosses) which help the correct identification of such phases[38]. The 80:20 w/w GMO/OA system with 20% of water and the 90:10 w/w Phyt/OA with 20% of water showed again a possibly hexagonal structure, while the 90:10 w/w Phyt/water system showed lamellar structure and the 80:20 w/w Phyt/water system exhibited an isotropic structure.

From the phase study it was concluded that the 80:20 w/w lipid/water ratio gave anisotropic structures for both systems while avoiding at the same time any phase separation in the gel. It was also concluded that 80:20 w/w GMO/OA and 90:10 w/w Phyt/OA ratios were likely to have hexagonal structures.

A.2 Ultrasonication tests

In order to find the most suitable ultrasonication dispersing method, different sonication parameters were tested. Dispersion methods found in literature [77, 43, 83] involving extrusion and filtering are not suitable for these systems containing peptides as a large amount of peptide could be withheld in the filter thus decreasing the efficiency of the drug loading. Methods involving high-pressure microfluidization could instead damage the peptide.
Effort were made into varying different sonication procedures. Two different ultrasonicators were used: a continuous SONIPREP 150 Ultrasonic Disintegrator (MSE Tamro Lab AB, Kungens Kurva, Sweden) and a pulsed Vibra-Cell VC 750 Ultrasonic processor (Sonics & Materials Inc., Newtown, USA). Also, parameters such as sonication time, pulse duration and frequency, dispersion volume, vial volume and temperature control were tested. The effectiveness of the method was assessed by measuring the temperature and the size distribution of the particles.

The continuous ultrasonicator tests on 80:20 GMO/OA w/w ratio and 75:25 Phyt/OA w/w ratio have proved to be promising. Narrow size distributions were obtained with a Z-average size between 110 and 145 nm and sonication times from 10 minutes to 20 minutes.
Temperatures were observed to reach almost 80°C, which excessively high for systems containing peptides which could be sensitive to elevated temperatures. A new batch of samples was immersed in an ice bath in order to set a better control of the temperature.
Unfortunately, size distributions of these samples were too wide suggesting that the ice bath hindered the sonication efficiency.
As a consequence a pulsed ultrasonicator was employed as the break time in between pulses would allow the heat to diffuse and keep the temperature stable. The use of a water bath was preferred for securing temperatures not higher than 40°C while avoiding at the same time an excessive cool down of the sample during sonication. The magnitude of the tip oscillation was set to 39%, the microtip being a 6 mm probe and the vials containing the solution had volume 14 ml. Excessively big vials would not allow the whole sample to be sonicated effectively.

The final choice for a sonication time was 5 minutes with 3 second pulses alternated with

7 second breaks as such a procedure would avoid the formation of an excessive amount of liposomes with the drawback of the presence of big agglomerates on the surface of the colloids which are described in Section 4.1.

Appendix B

Additional data

B.1 Polarized light microscopy

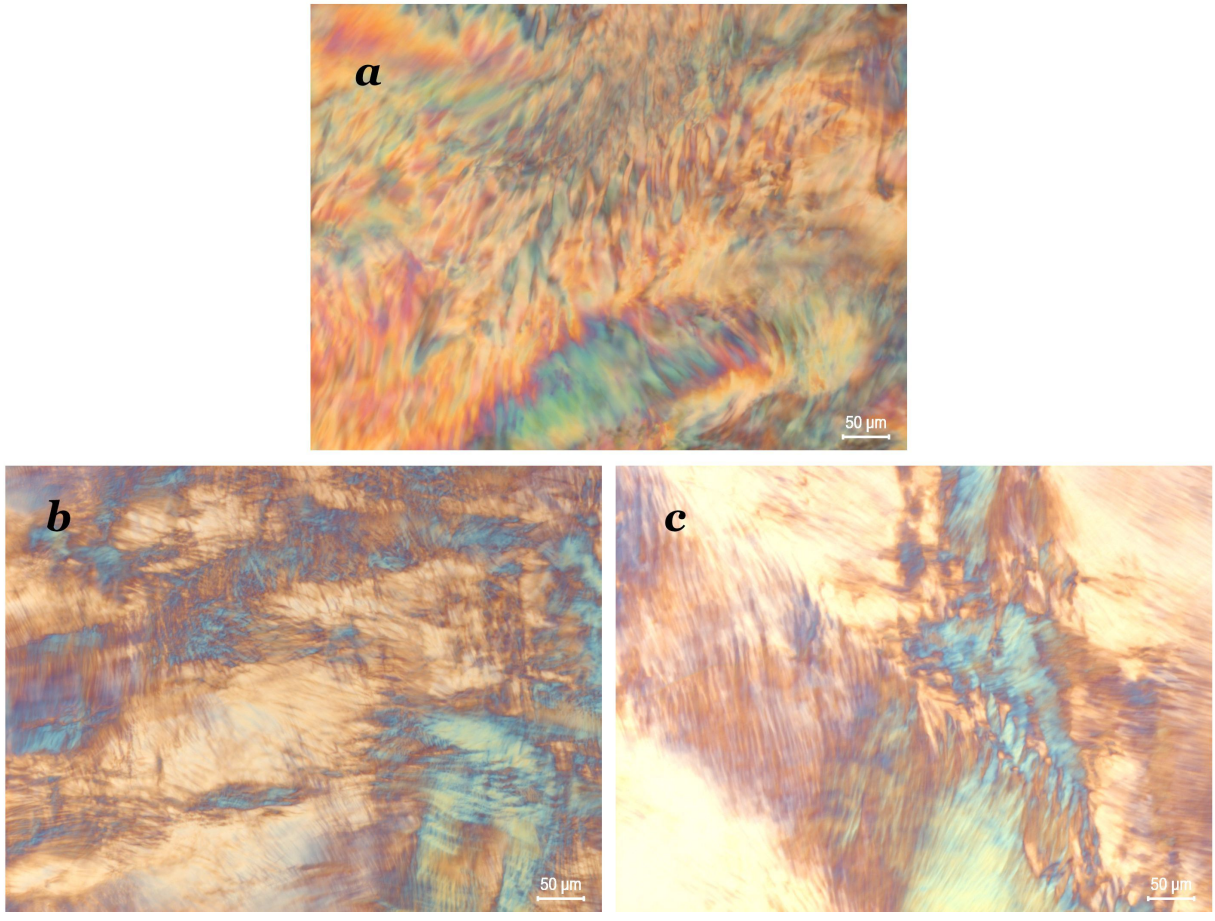

Figure B.1.1: *Polarized microscopy images with λ plate. a)Unloaded 80:20 GMO/OA bulk phase; a)80:20 GMO/OA bulk phase loaded with DPK-060; a)80:20 GMO/OA bulk phase loaded with AP114.*

B.2 Particle size determination and stability

Table B.2.1: *Unloaded samples' Z-average particle size.*

Phyt/OA	Particle size [nm]	PDI
70:30	319,6±4,0	0,451±0,02
75:25	348,9±1,5	0,397±0,03
80:20	323,86±7,0	0,39±0,01
90:10	270,6±2,0	0,285±0,02
GMO/OA	Particle size [nm]	PDI
80:20	130,2±1,2	0,307±0,005
85:15	178,36±1,8	0,151±0,015
90:10	137,46±1,2	0,202±0,005
95:5	164,23±1,2	0,135±0,03

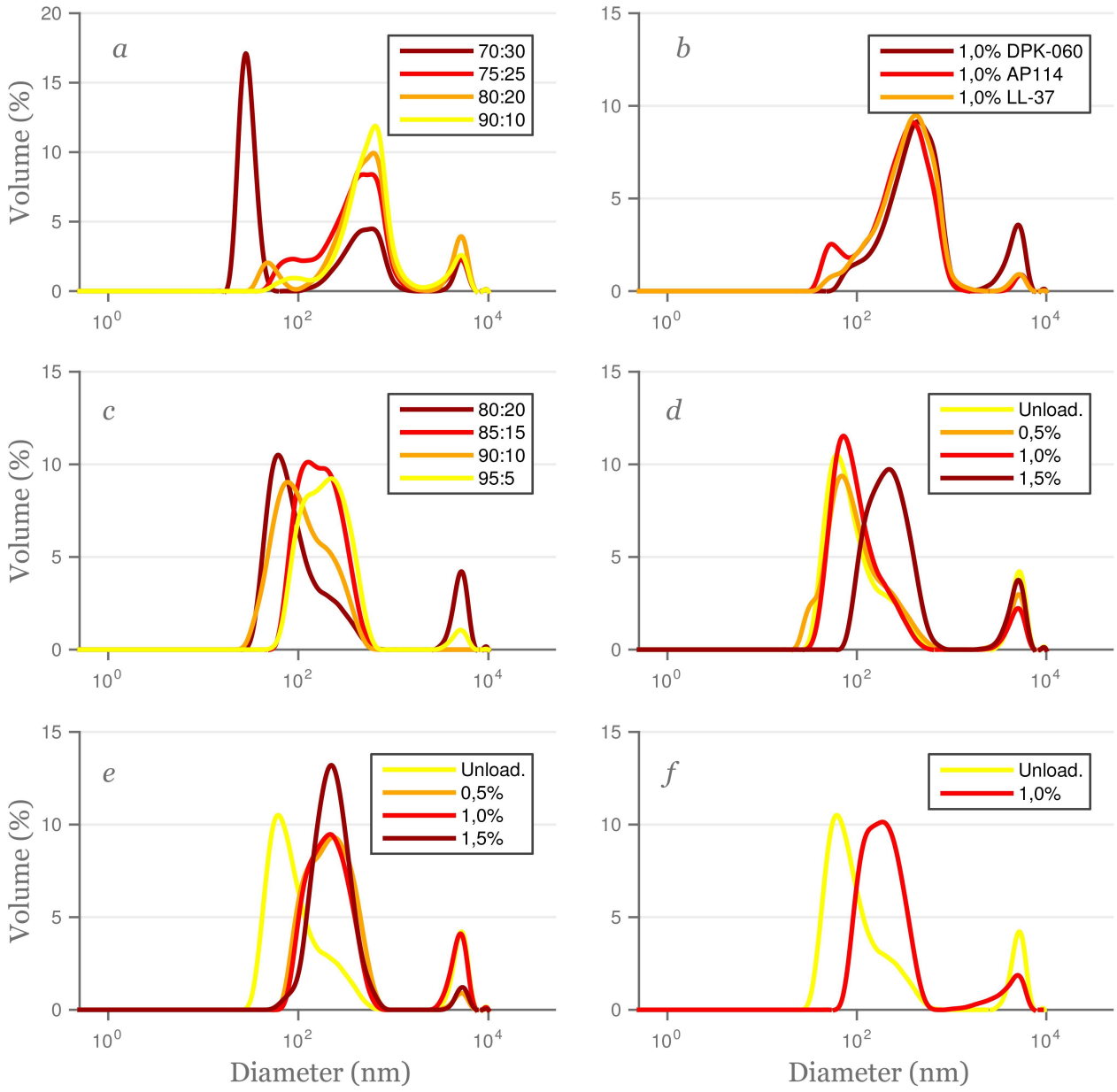

Figure B.2.1: *Particle size diameter 4 days after preparation. a)Phyt/OA; b)Loaded 90:10 Phyt/OA; c)GMO/OA; d)80:20 GMO/OA loaded with DPK-060; e)80:20 GMO/OA loaded with AP114; f)80:20 GMO/OA loaded with LL-37.*

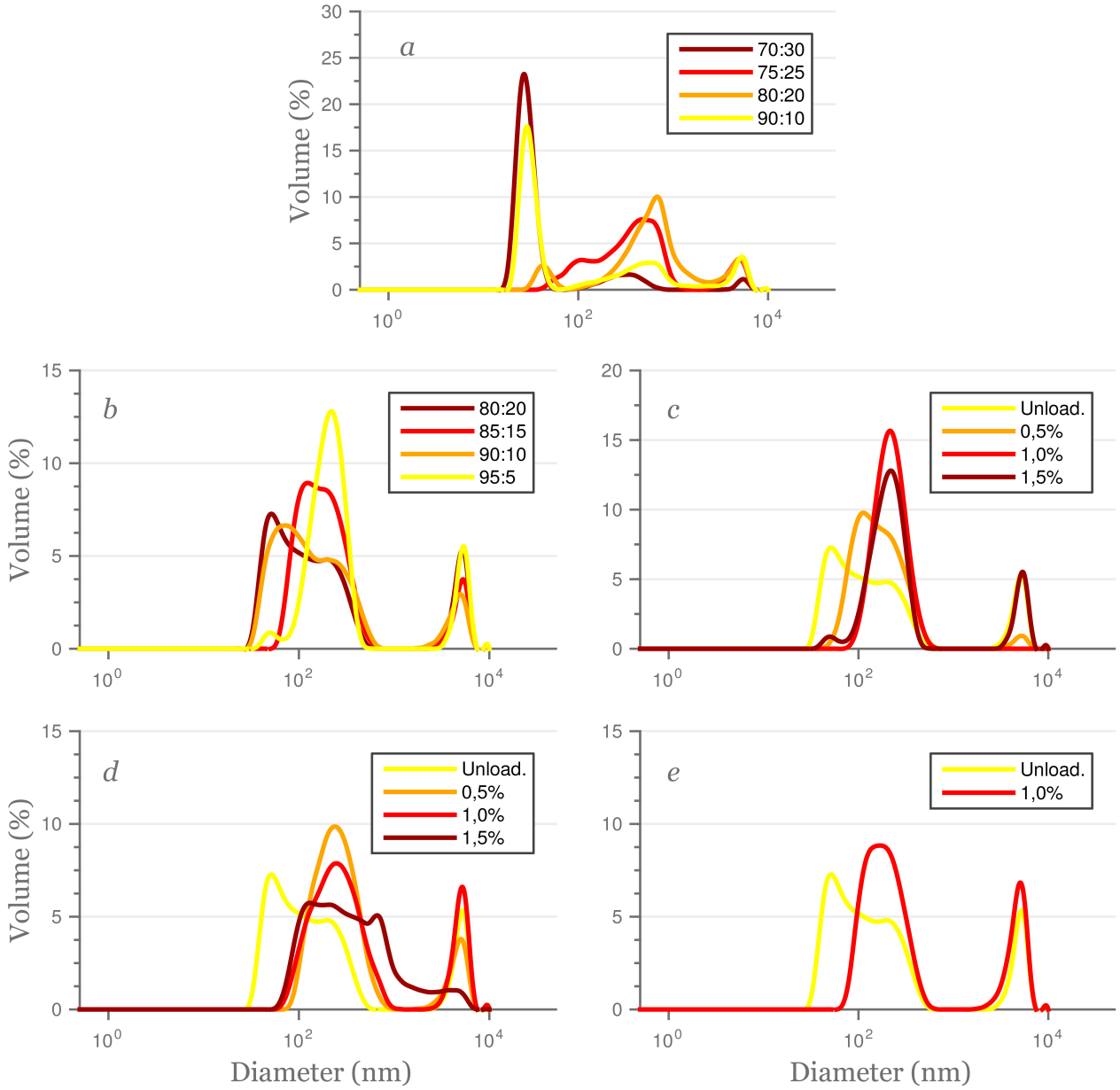

Figure B.2.2: *Particle size diameter 40 days after preparation. a)Phyt/OA; b)GMO/OA; c)80:20 GMO/OA loaded with DPK-060; d)80:20 GMO/OA loaded with AP114; e)80:20 GMO/OA loaded with LL-37.*

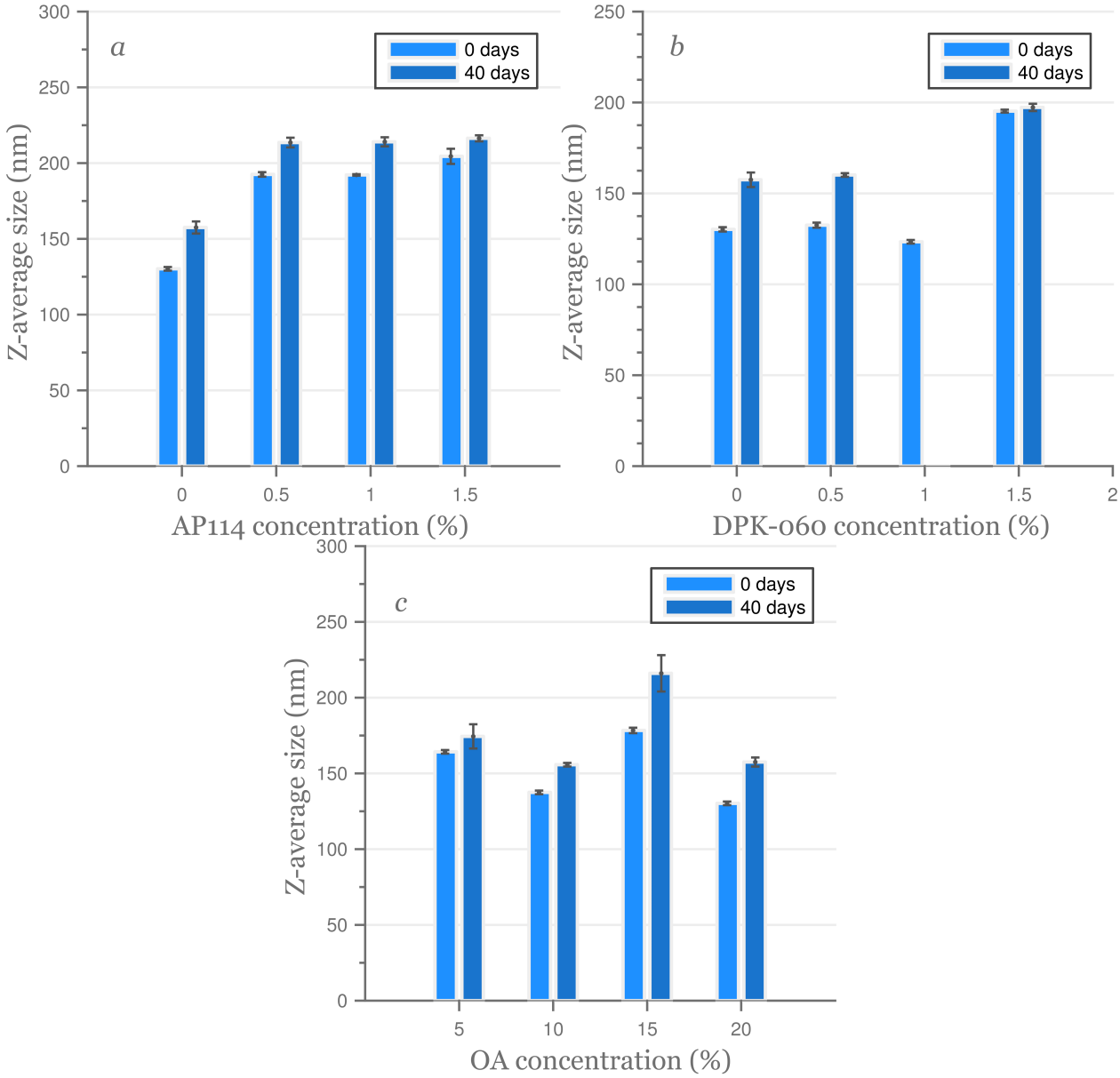

Figure B.2.3: *Z-average particle size increase in 40 days. a)80:20 GMO/OA loaded with AP114; b)80:20 GMO/OA loaded with DPK-060; c)Unloaded 80:20 GMO/OA.*

B.3 Peptide net charge

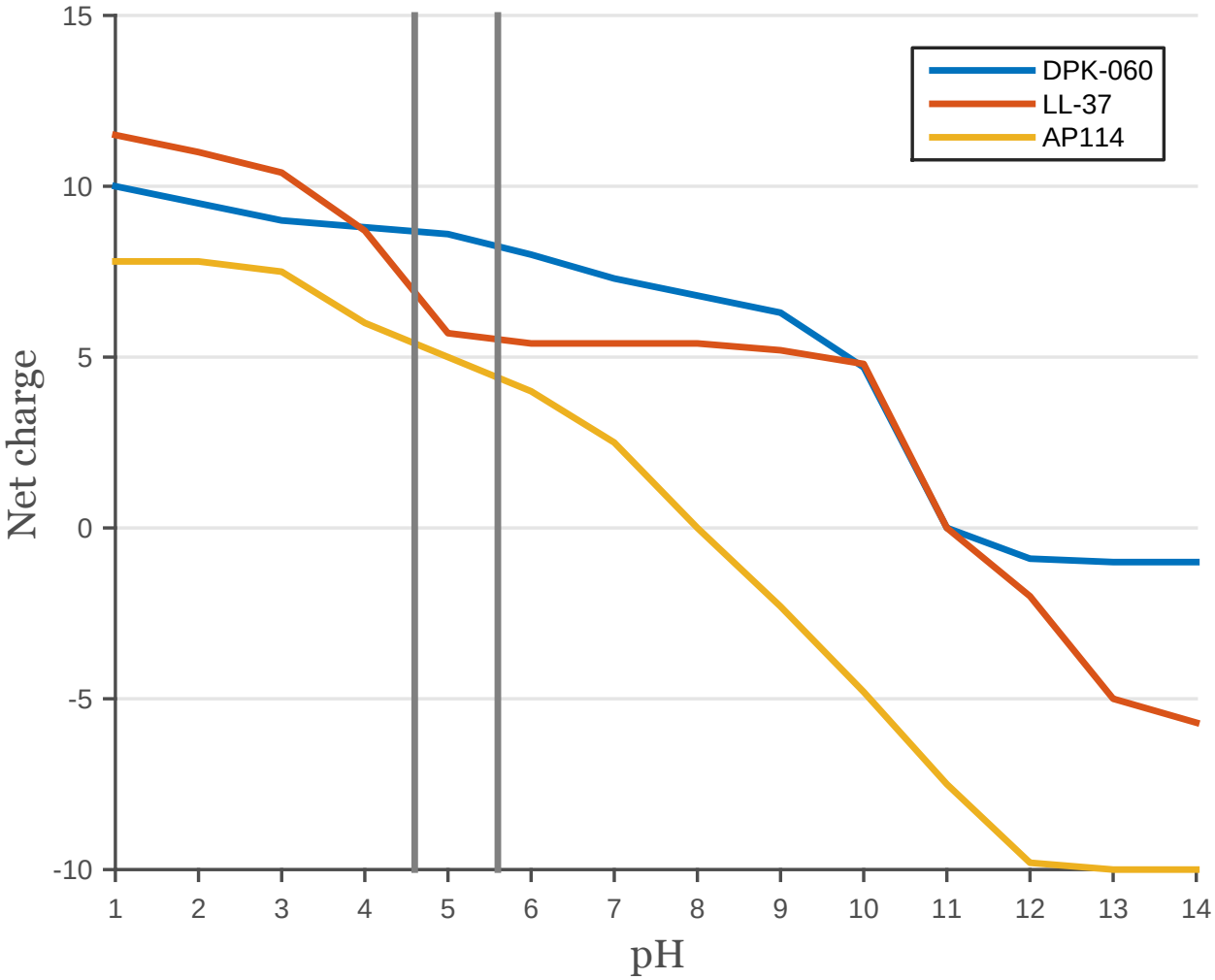

Figure B.3.1: *Net charge vs pH of the DPK-060, LL-37 and AP114 peptides. The area enclosed by the two vertical lines is the region of interest.*

B.4 Zeta potential

Table B.4.1: *Zeta potentials of unloaded samples.*

GMO/OA	Zeta potential [mV]	Phyt/OA	Zeta potential [mV]
80:20	-33,8±1,3	90:10	-25,63±0,8
85:15	-33,46±0,4	80:20	-30,87±1,0
90:10	-26,5±1,0	75:25	-25±1,0
95:5	-29,63±0,8	70:30	-25,47±0,4

Table B.4.2: *Zeta potentials and pH values of 80:20 GMO/OA samples loaded with peptide.*

GMO/OA	Peptide	Peptide conc. [%]	pH	Zeta potential [mV]
80:20	-	-	5,30	-33,8±1,3
80:20	AP114	0,5	5,00	-24,83±0,3
80:20	AP114	1,0	4,81	-23,1±1,0
80:20	AP114	1,5	4,66	-19,63±1,4
80:20	DPK-060	0,5	5,10	-31,13±0,4
80:20	DPK-060	1,0	4,96	-21,06±0,6
80:20	DPK-060	1,5	4,72	-21,3±0,1
80:20	LL-37	1	-	-24,06±1,0

Table B.4.3: *Zeta potentials and pH values of 90:10 Phyt/OA samples loaded with peptide.*

Phyt/OA	Peptide	Peptide conc. [%]	pH	Zeta potential [mV]
90:10	-	-	5,40	-25,63±0,8
90:10	AP114	1,0	5,03	-9,46±0,15
90:10	DPK-060	1,0	4,97	-19,5,1±0,2
90:10	LL-37	1,0	5,09	-18,43±0,3

Table B.4.4: *Zeta potentials and pH values of 80:20 GMO/OA samples loaded with peptide diluted in acetate buffer.*

GMO/OA	Peptide	Peptide conc. [%]	pH	Zeta potential [mV]
80:20	-	-	5,6	-4,56±0,2
80:20	AP114	0,5	5,61	-5,13±0,1
80:20	AP114	1,0	5,56	-0,4±0,4
80:20	AP114	1,5	5,51	-0,01±0,5

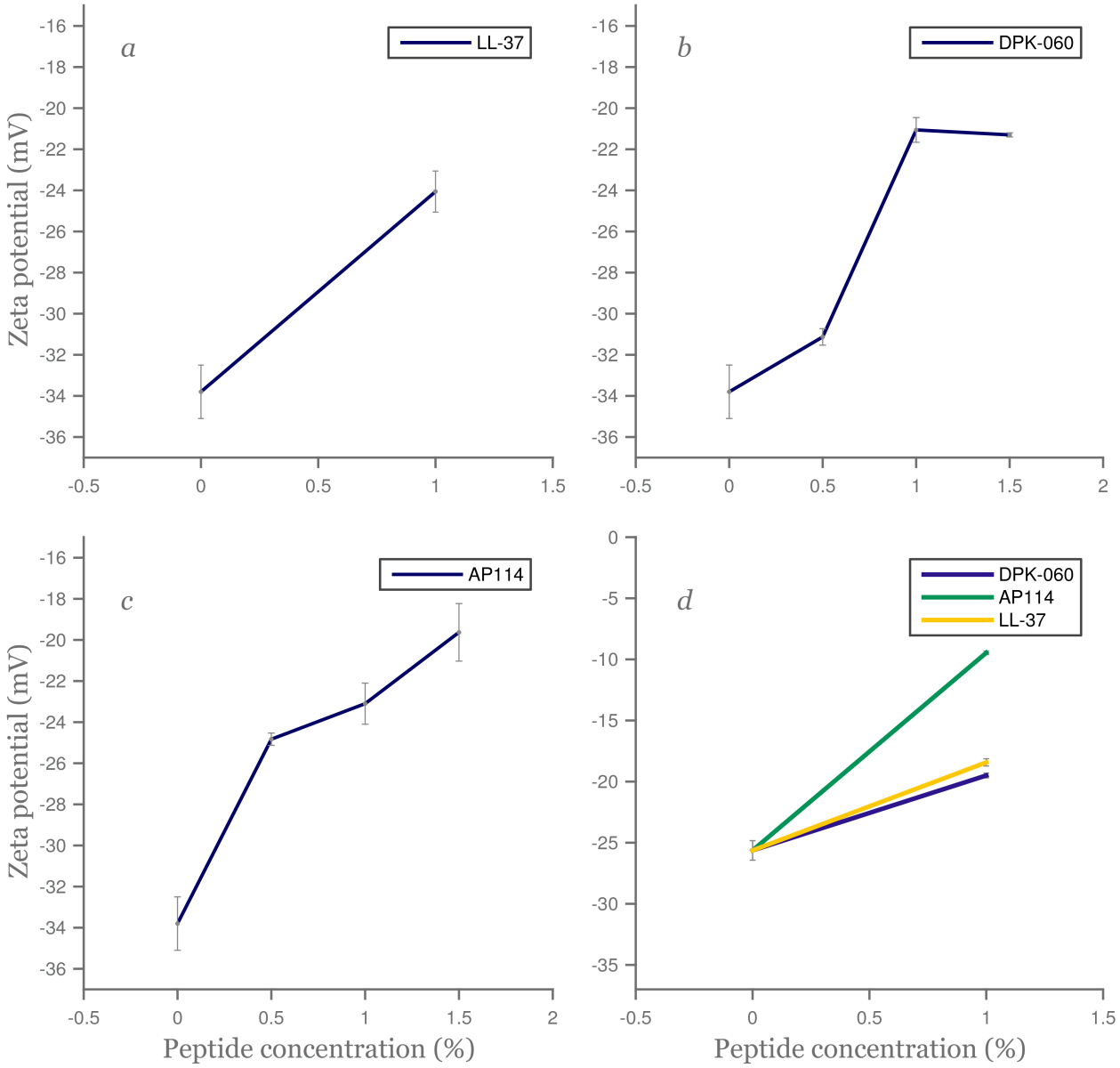

Figure B.4.1: *Zeta potentials vs. peptide concentration. a)80:20 GMO/OA loaded with LL-37; b)80:20 GMO/OA loaded with DPK-060; c)80:20 GMO/OA loaded with AP114; d)90:10 Phyt/OA.*

B.5 Small Angle X-ray Scattering (SAXS)

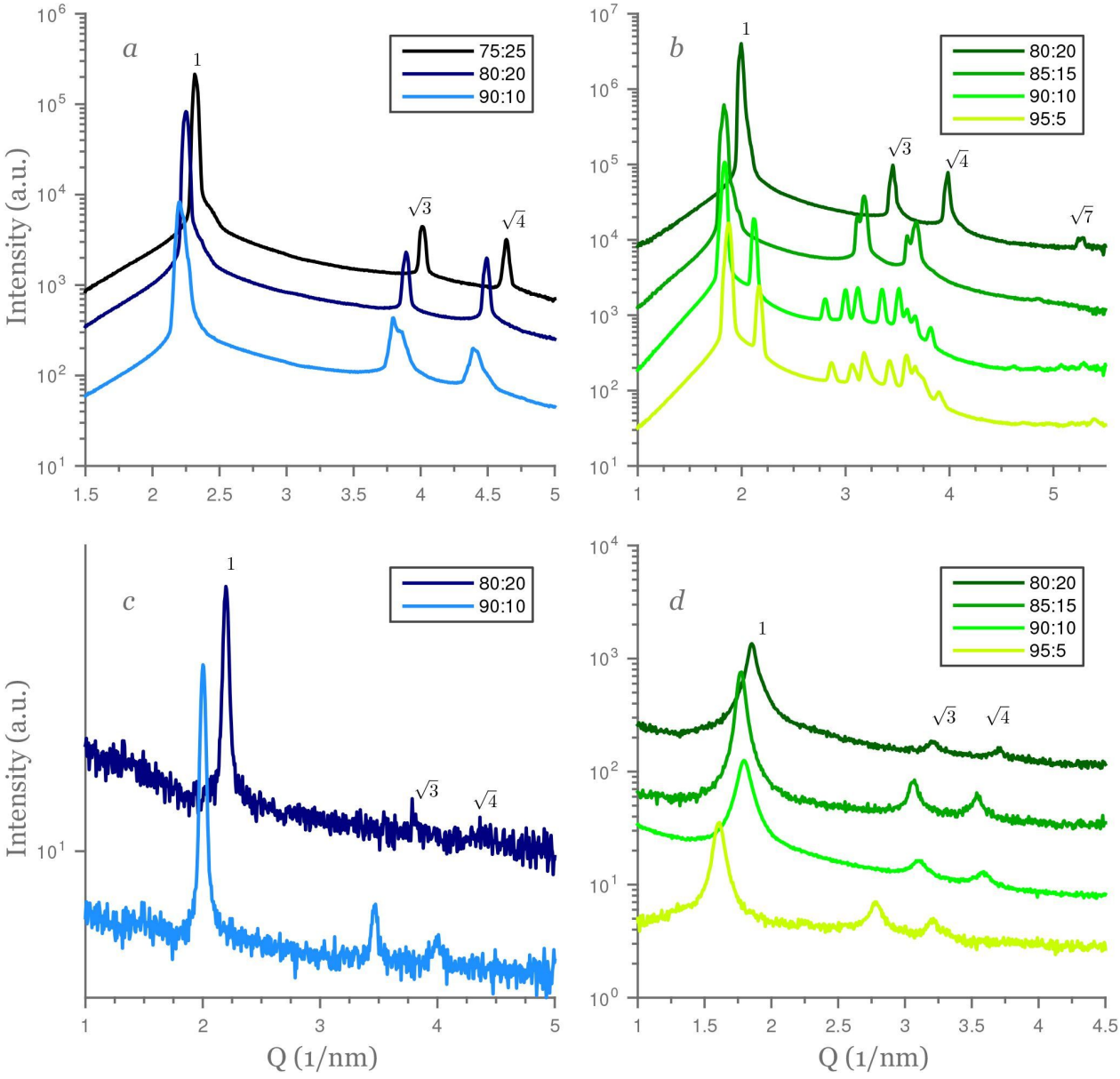

Figure B.5.1: *SAXS diffractograms of unloaded samples. a)Phyt/OA bulk phases; b)GMO/OA bulk phases; c)Phyt/OA dispersed phases; d)GMO/OA dispersed phases.*

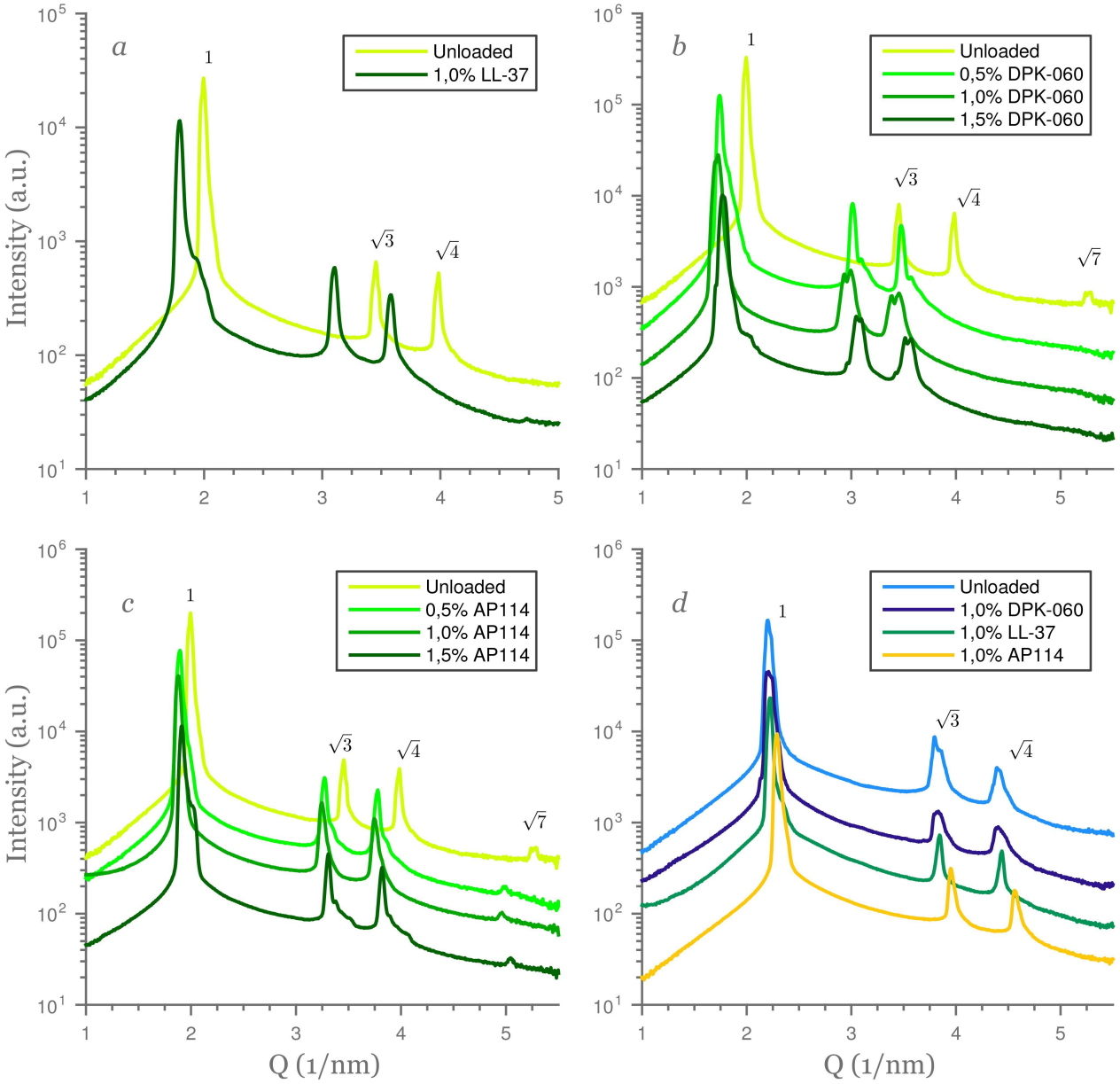

Figure B.5.2: *SAXS diffractograms of bulk phases. a)80:20 GMO/OA loaded with LL-37; b)80:20 GMO/OA loaded with DPK-060; c)80:20 GMO/OA loaded with AP114; d)90:10 Phyt/OA loaded with selected peptides.*

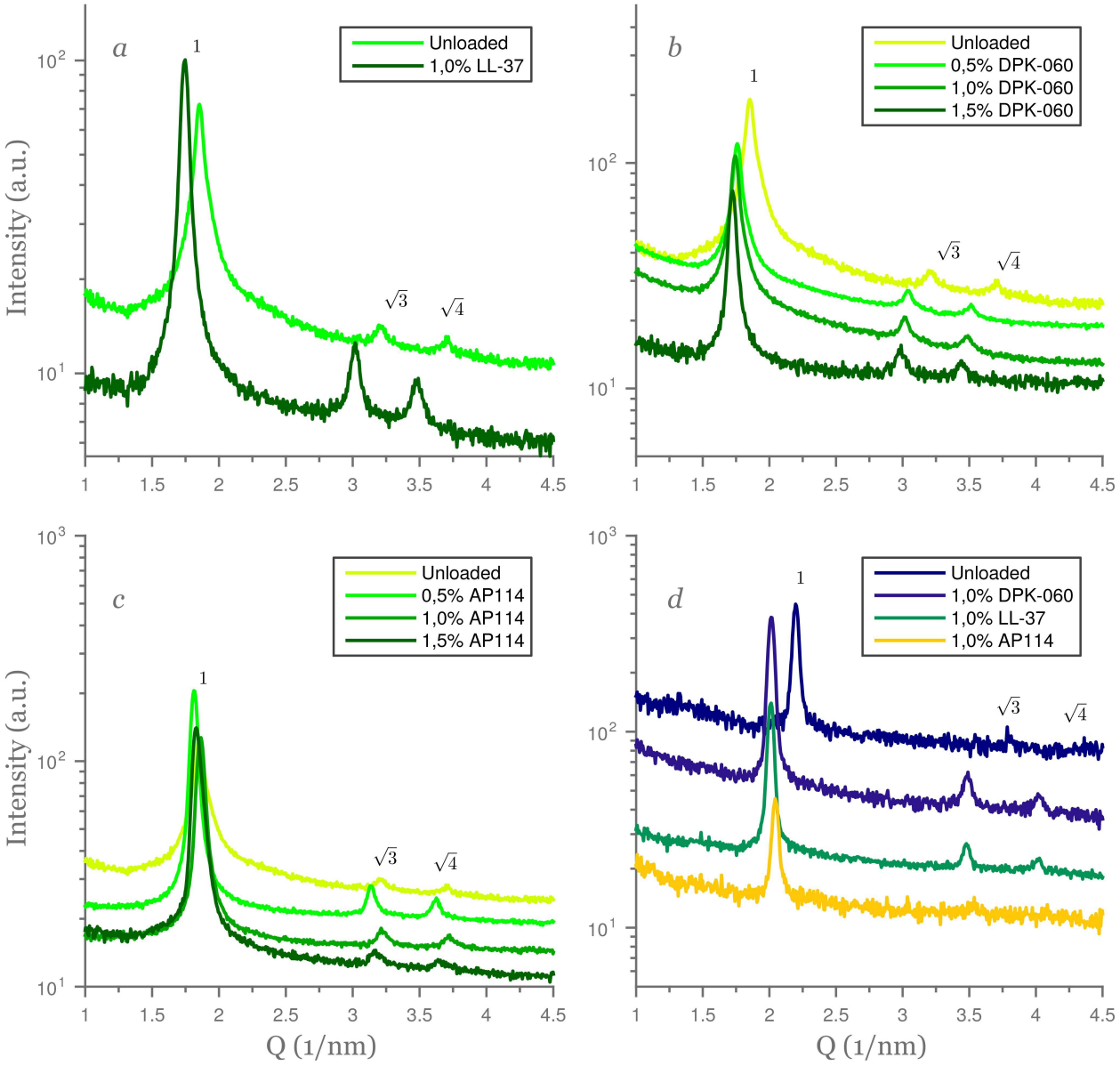

Figure B.5.3: *SAXS diffractograms of dispersed phases. a)80:20 GMO/OA loaded with LL-37; b)80:20 GMO/OA loaded with DPK-060; c)80:20 GMO/OA loaded with AP114; d)90:10 Phyt/OA loaded with selected peptides.*

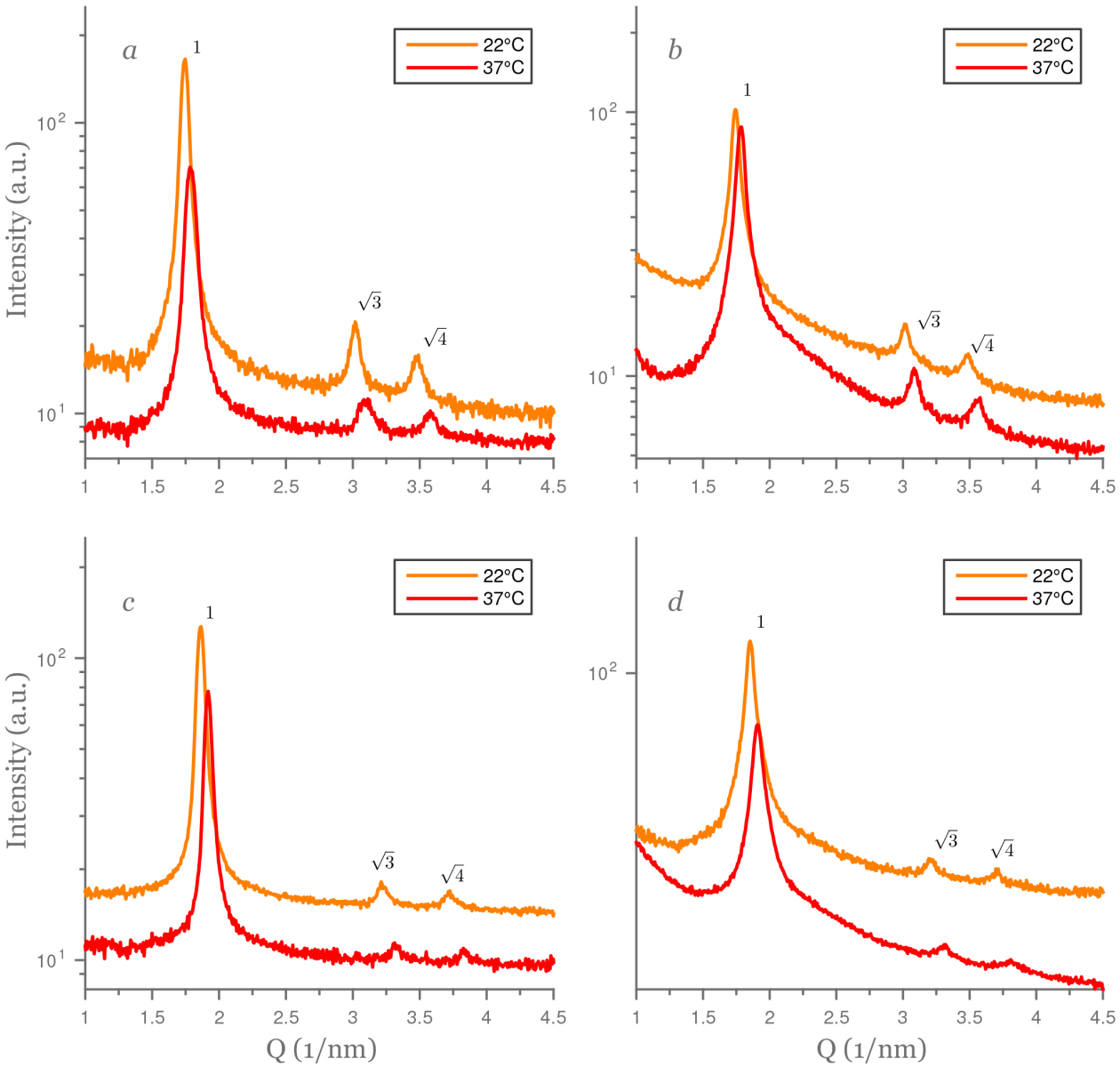

Figure B.5.4: *SAXS diffractograms of dispersed phases at 37°C. a)80:20 GMO/OA loaded with LL-37; b)80:20 GMO/OA loaded with DPK-060; c)80:20 GMO/OA loaded with AP114; d)Unloaded 80:20 GMO/OA.*

TRITA TRITA-ICT-EX-2015:100